THESIS APPROVAL

GRADUATE SCHOOL, KASETSART UNIVERSITY

Master of Engineering (Materials Engineering)

DEGREE

Materials Engineering	Materials Engineering
FIELD	**DEPARTMENT**

TITLE: Preparation of Rare Earth-doped Ceria Powders from Metal Complex Used as An Electrolyte in Solid Oxide Fuel Cells

NAME: Mr. Thamrong Rakthin

THIS THESIS HAS BEEN ACCEPTED BY

_____ **THESIS ADVISOR**

(Assistant Professor Apirat Laobuthee, Ph.D. **)**

_____ **THESIS CO-ADVISOR**

(Assistant Professor Nattamon Koonsaeng, Ph.D. **)**

_____ **THESIS CO-ADVISOR**

(Associate Professor Navadol Laosiripojana, Ph.D. **)**

_____ **DEPARTMENT HEAD**

(Assistant Professor Wisit Locharoenrat, M.S. **)**

APPROVED BY THE GRADUATE SCHOOL ON _____

_____ **DEAN**

(Associate Professor Gunjana Theeragool, D.Agr. **)**

THESIS

PREPARATION OF RARE EARTH-DOPED CERIA POWDERS FROM METAL COMPLEX USED AS AN ELECTROLYTE IN SOLID OXIDE FUEL CELLS

THAMRONG RAKTHIN

A Thesis Submitted in Partial Fulfillment of
the Requirements for the Degree of
Master of Engineering (Materials Engineering)
Graduate School, Kasetsart University
2009

Thamrong Rakthin 2009: Preparation of Rare Earth-doped Ceria Powders from Metal Complex Used as An Electrolyte in Solid Oxide Fuel Cells. Master of Engineering (Materials Engineering), Major Field: Materials Engineering, Department of Materials Engineering. Thesis Advisor: Assistant Professor Apirat Laobuthee, Ph.D. 82 pages.

CeO_2, $Ce_{1-x}Gd_xO_{2-\delta}$, and $Ce_{1-x}Sm_xO_{2-\delta}$ (where x = 0.10, 0.15, and 0.20) powders can be prepared via metal complex method. This method offers the advantages of easy, inexpensive, and straightforward to produce high purity and homogeneity products. Based on FTIR and ESI-MS techniques, two possible structures of cerium complexes can be proposed as four coordinated cerium ion binding to TEA molecule [Ce(TEA)] and five coordinated cerium ion with TEA and Cl^- ligands [Ce(TEA)Cl). In addition, doped cerium complexes can be prepared via metal complex method. The TGA/DSC results showed that the appropriate temperature for calcining metal complexes into ceramic powders is started at 600°C. The effect of calcination temperatures revealed that the crystallite size and average particle size are increased with increasing calcination temperature while specific surface area decreased. From impedance spectroscopy, $Ce_{0.85}Gd_{0.15}O_{2-\delta}$ and $Ce_{0.90}Sm_{0.10}O_{2-\delta}$ give the largest ionic conductivity as 0.0302 and 0.0284 S/cm, respectively.

_____ _____ __ / __ / __

Student's signature Thesis Advisor's signature

ACKNOWLEDGEMENTS

I would like to grateful thank and deeply indebted to Asst. Prof. Dr. Apirat Labuthee my thesis advisor for advice, encouragement, and valuable suggestion for completely working of thesis. I would sincerely like to thank Asst. Prof. Dr. Nattamon Koonsaeng, and Assoc. Prof. Dr. Navadol Laosiripojana my thesis committees, and also Assoc. Prof. Dr. Vanida Bhavakul from Graduate School for their valuable comments and suggestions.

I would like to sincerely thank Dr. Chatchai Veranitisagul for his suggestion, encouragement and enthusiasm during study and research work. I would like to also thank Assoc. Prof. Dr. Sutin Kuharuangrong (School of Ceramic Engineering, Suranaree University of Technology) for electrical measurement, Ms. Wannee Srinutrakul (Thailand Institute of Nuclear Technology (TINT)) for surface area analysis. I would like to acknowledge Mettler Toledo (Thailand) Limited for TGA/DSC analysis, Thailand Institute of Scientific and Technological Research (TISTR) for pellet sample preparation, and Thailand Institute of Nuclear Technology (TINT) for X-ray diffraction analysis. I am heartfelt thank to my friends; Mr. Attaphon Kaewvilai, Mr. Sarawut Sangngern, Mr. Sarute Ummartyotin, Mr. Thammanoon Thaweechai, and all of members in my laboratory for giving me helps, good time and good memories during study and research work.

This research was supported by Energy Policy and Planning Office (EPPO), Ministry of Energy, Thailand and partially funded by Kasetsart University Research and Development Institute (KURDI), Faculty of Engineering, Kasetsart University, Thailand.

Finally, I am especially appreciated my parent, my sisters and brothers for their love, understanding, and continuing encouragements.

Thamrong Rakthin

April, 2009

TABLE OF CONTENTS

Page

LIST OF TABLES

LIST OF FIGURES

LIST OF FIGURES (Continued)

LIST OF FIGURES (Continued)

Figure **Page**

Appendix Figure

LIST OF FIGURES (Continued)

LIST OF ABBREVIATIONS

AFC	=	Alkaline Fuel Cell
DMFC	=	Direct Methanol Fuel Cell
PAFC	=	Phosphoric Acid Fuel Cell
SAFC	=	Sulfuric Acid Fuel Cell
PEMFC	=	Proton Exchange Membrane Fuel Cell
MCFC	=	Molten Carbonate Fuel Cell
SOFC	=	Solid Oxide Fuel Cell
OOPS	=	Oxide One Pot Synthesis
FTIR	=	Fourier transform infrared spectroscopy
ESI-MS	=	Electrospray ionization-mass spectroscopy
TGA	=	Thermogravimetric analysis
DSC	=	Differential scanning calorimetry
BET	=	Brunauer-Emmett-Teller
XRD	=	X-ray diffraction
SEM	=	Scanning electron microscope
EIS	=	Electrochemical impedance spectroscopy
CIP	=	Cold isostatic pressing
YSZ	=	Yttria-stabilized zirconia
LSM	=	Lanthanum strontium manganite
LSCF	=	Lanthanum strontium cobalt ferrite
PEG	=	Polyethylene glycol
TEA	=	Triethanolamine
CTE	=	Coefficient of thermal expansion
MIEC	=	Mixed ionic/electronic conducting
°C	=	Degree celsius
h	=	hour
min	=	minute
M	=	Molar
%	=	Percentage

LIST OF ABBREVIATIONS (Continued)

S/cm	=	Siemens per centimeter
cm^{-1}	=	Per centimeter
m/z	=	Mass per charge
nm	=	Nanometer
θ	=	Theta
JCPDS	=	Joint Committee on Powder Diffraction Standards
K	=	Kelvin
m^2/g	=	Square meter per gram
g/cm^3	=	Gram per cubic centimeter
kV	=	Kilovolt
MPa	=	Megapascal
°	=	Degree
D	=	Dry weight
W	=	Saturated weight
S	=	Suspended weight
ρ	=	Density of water
Hz	=	Hertz
MHz	=	Megahertz
R	=	Resistance
L	=	Thickness
A_e	=	Area of the electrode
σ	=	Electrical conductivity
T	=	Temperature
A	=	Pre-exponential factor
E_a	=	Activation energy
k	=	Boltzmann's constant
pH	=	Percent of hydrogen ion
D_{XRD}	=	Crystallite size
S_{BET}	=	Specific surface area

LIST OF ABBREVIATIONS (Continued)

D_{BET}	=	Average particle size
K^{-1}	=	Per Kelvin
$Scm^{-1}K$	=	Siemens Kelvin per Centimeter
σ_b	=	Bulk conductivity
σ_{gb}	=	Grain boundary conductivity
σ_t	=	Total conductivity
eV	=	Electron volt
IT-SOFCs	=	Intermediate temperature-solid oxide fuel cells

PREPARATION OF RARE EARTH-DOPED CERIA POWDERS FROM METAL COMPLEX USED AS AN ELECTROLYTE IN SOLID OXIDE FUEL CELLS

INTRODUCTION

Nowadays, many countries have been seriously concerned about air pollution (especially from fossil fuel energies) which produced some greenhouse gas (mainly CO_2), resulting in the existence of climate change. Therefore, there are many efforts to discover and develop new power generation technologies.

Fuel cells are one promising technology as a candidate alternative power generation technology. A key feature of fuel cells is its high energy conversion efficiency. They can convert the chemical energy of the fuels (hydrogen, methane, butane, or gasoline and diesel) into electrical energy by the electrochemical process. As comparing with other power generation technologies, fuel cells offer several advantages of substantially higher conversion efficiency, modular construction, high efficiency at part load, minimal site restriction, potential for cogeneration, and much lower production of pollutants (Boudghene and Traversa, 2002).

Fuel cells consist of two electrodes (anode and cathode) separated by an electrolyte. Individual fuel cells are, therefore, connected in electrical series as a stack by a bipolar plate or interconnect to produce the useful power. The operating principles of fuel cells are similar to those of batteries, i.e., electrochemical combination of reactants to generate electricity, a combination made of a gaseous fuel (hydrogen) and an oxidant gas (O_2 from the air) through electrodes and via an ion conducting electrolyte. Unlike the batteries, the fuel cells cannot be run down or recharged. Moreover, the fuel cells operate as long as both fuel and oxidant are supplied to the electrodes (Minh, 1993).

Several types of fuel cells are generally classified by electrolyte used as an ionic conductor in the cell, i.e., Alkaline Fuel Cell (AFC), Direct Methanol Fuel Cell (DMFC), Phosphoric Acid Fuel Cell (PAFC), Sulfuric Acid Fuel Cell (SAFC), Proton Exchange Membrane Fuel Cell (PEMFC), Molten Carbonate Fuel Cell (MCFC), Solid Oxide Fuel Cell (SOFC), and etc. Among all type of fuel cells, SOFCs has been much attention to develop. In the fact that they are able to convert a wide variety of fuels and exhibit the highest efficiency compared to engines and modern thermal plants.

SOFCs are composed of all four main components; electrolyte, anode, cathode, and interconnect. Stabilized zirconia (ZrO_2), especially yttria-stabilized zirconia (YSZ), the most common electrolyte, possesses an adequate level of oxygen ion conductivity and exhibits desirable stability in both oxidizing and reducing atmospheres. In addition, nickel/stabilized zirconia cermet, doped lanthanum manganite, and doped lanthanum chlomite are used for anode, cathode, and interconnect, respectively. However, the operating temperature of SOFCs is around 1000°C, resulting in various phenomena, such as chemical reaction between components, thermal degradation, and thermal expansion mismatch of materials or cracking during the processes. Many researches have, therefore, aimed to reduce the operating temperature of SOFCs. To solve the problem, the new materials with high ionic conductivity have been developed to replace the YSZ electrolyte.

Doped ceria is an interesting oxide material that becomes for replacing YSZ. Aliovalent dopants, such as rare earth oxides (Gd_2O_3, Sm_2O_3, Nd_2O_3, etc) can form solid solutions with ceria ($Ce_{1-x}Re_xO_{2-\delta}$, where Re = rare earth) and introduce oxygen ion vacancies which are responsible for the ionic conductivity observed. Due to the high ionic conductivity at moderate temperature (~600-800°C), the doped ceria was considered as a candidate electrolyte in intermediate temperature solid oxide fuel cells (IT-SOFCs).

Up to now, there are several synthesis routes used to prepare ceria and doped ceria powders. In the investigation of electrolyte material for SOFCs, the component

compositions always need to be adjusted, so finding and selecting a simple and low cost but effective method to prepare doped ceria powder has distinct advantages for SOFCs research.

By the oxide one pot synthesis (OOPS) process, Laobuthee *et al.* successfully prepared magnesium aluminate ($MgAl_2O_4$) powder from metal complex. This method offers the advantages of low cost, straightforward and very simple to provide high purity and homogeneity products. In addition, the obtained $MgAl_2O_4$ exhibited good humidity sensitivity as comparing to that prepared via other methods (Laobuthee et al., 2000). Thus, goal of this work is to develop the OOPS process to prepare ceria and doped ceria powders. It is well known that OOPS process required the high reaction temperature to complete the reaction to obtain the metal complex because the reaction is operated using ethylene glycol as solvent for metal oxide starting materials. To reduce the reaction temperature, in this research work, the OOPS process was develop to prepare ceria and doped ceria powders. The metal complexes were synthesized from metal chloride salts and a simple organic ligand as triethanolamine. The low boiling point solvent as propan-1-ol was used to reduce the reaction temperature. To determine the possible structures of metal complexes, FTIR and ESI-MS techniques were used to characterize the obtained metal complexes. Thermal properties of metal complexes were carried out by TGA/DSC. The ceramic powders from various calcination temperatures were studied by XRD, BET and SEM. In addition, the ionic conductivity of doped ceria pellets was examined by impedance spectroscopy.

OBJECTIVES

1. To develop the OOPS process to prepare CeO_2, $Ce_{1-x}Gd_xO_{2-\delta}$, and $Ce_{1-x}Sm_xO_{2-\delta}$ powders from the metal chloride salts.

2. To study the electrical properties of the obtained $Ce_{1-x}Gd_xO_{2-\delta}$ and $Ce_{1-x}Sm_xO_{2-\delta}$.

LITERATURE REVIEW

1. Fuel Cells

Fuel cells are an electrochemical device that converts the chemical energy in fuels (such as hydrogen, methane, butane or even gasoline and diesel) into electrical energy. A fuel cell consists of two electrodes (the anode and cathode) separated by electrolyte, as shown in Figure 1.

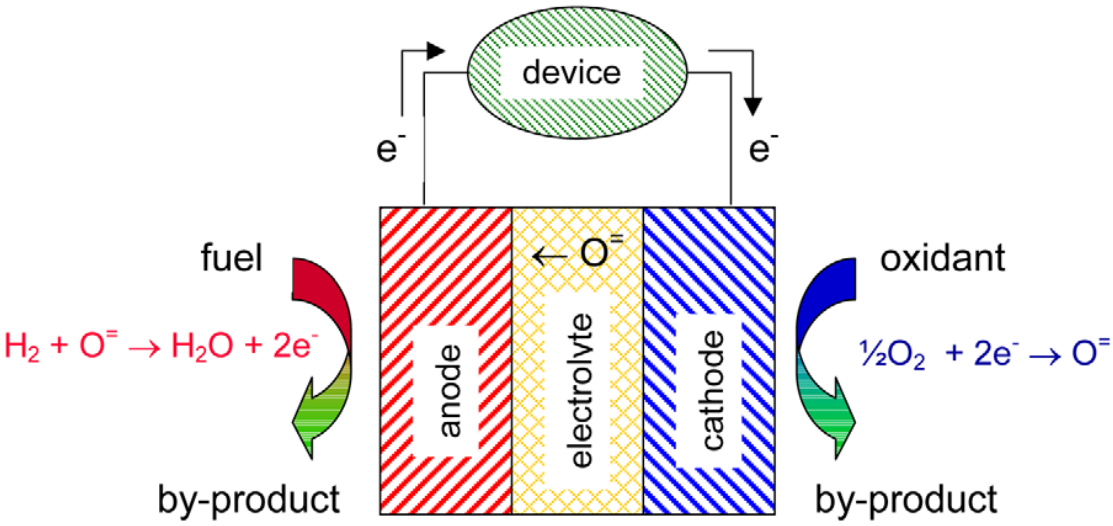

Figure 1 The schematic of a fuel cell

Source: Haile (2003)

Fuel (e.g., H_2) is fed to the anode and oxidized while electrons are released to the external (outer) circuit. Oxidant (e.g., O_2) is fed to the cathode and reduced while electrons are accepted for the external circuit. The electrons flow (from the anode to the cathode) through the external circuit producing the direct-current electricity. The electrolyte conducts ions between the two electrodes.

Practical fuel cells are not operated as a single unit. A series of cells referred to as a stack are used to generate the electricity. A component, variously called a

bipolar separator or an interconnect, connects the anode of one cell to the cathode of the next cell in a stack. Fuel cell stacks can be configured in series, parallel, both series and parallel, or as single units, depending on the particular application. (Minh N.Q., 1993)

Generally, fuel cells are considered as an environmental friendly power source because of no need of the direct combustion as an intermediate step during operation. Its conversion efficiency is not subjected to the Carnot limitation, resulting in the only releasing of heat and water-by product. Fuel cells can operate virtually continuously as long as the necessary flow of fuel and oxidant are maintained. They are different from electrochemical cell batteries in that they consume reactant, which must be replenished, whereas batteries store electrical energy chemically in a closed system. Additionally, the electrodes within battery react and change as a battery charged or discharged but fuel cells electrodes are catalytic and relatively stable.

Fuel cells are very useful as power sources in remote locations, such as spacecraft, remote weather stations, large parks, rural location, and in certain military applications. In addition, fuel cells can be applied for micro-combined heat and power systems such as home fuel cells and cogeneration for office buildings and factories are in mass production phase.

Several types of fuel cells classified by the chemical characteristics of the electrolyte used as ionic conductor are summarized in Table 1.

Table 1 Types of fuel cells and their operating conditions

Type of Fuel Cells	Electrolyte	Operating Temperature	Fuel	Oxidant	Efficiency
AFC	KOH	50-200°C	pure H_2 or N_2H_4	O_2/Air	50-55%
DMFC	polymer	60-200°C	liquid MeOH	O_2/Air	40-55%
PAFC	H_3PO_4	160-210°C	H_2 from hydrocarbon and alcohol	O_2/Air	40-50%
SAFC	H_2SO_4	80-90°C	alcohol or impure H_2	O_2/Air	40-50%
PEMFC	polymer, proton exchange membrane	50-80°C	less pure H_2 from hydrocarbon or MeOH	O_2/Air	40-50%
MCFC	Molten salts such as nitrate, sulphate, carbonate	630-650°C	H_2, CO, natural gas, propane, marine diesel	CO_2/O_2/Air	50-60%
SOFC	YSZ, doped CeO_2 or doped perovskite	600-1000°C	natural gas or propane	O_2/Air	45-60%

2. The Solid Oxide Fuel Cells (SOFCs)

SOFCs are composed of all-solid-state materials while other fuel cells make from both solid and liquid materials. SOFCs are generally operated at temperature ~1000°C, which is higher temperature than any other fuel cells. The schematic diagram of the operation in SOFCs is illustrated in Figure 2.

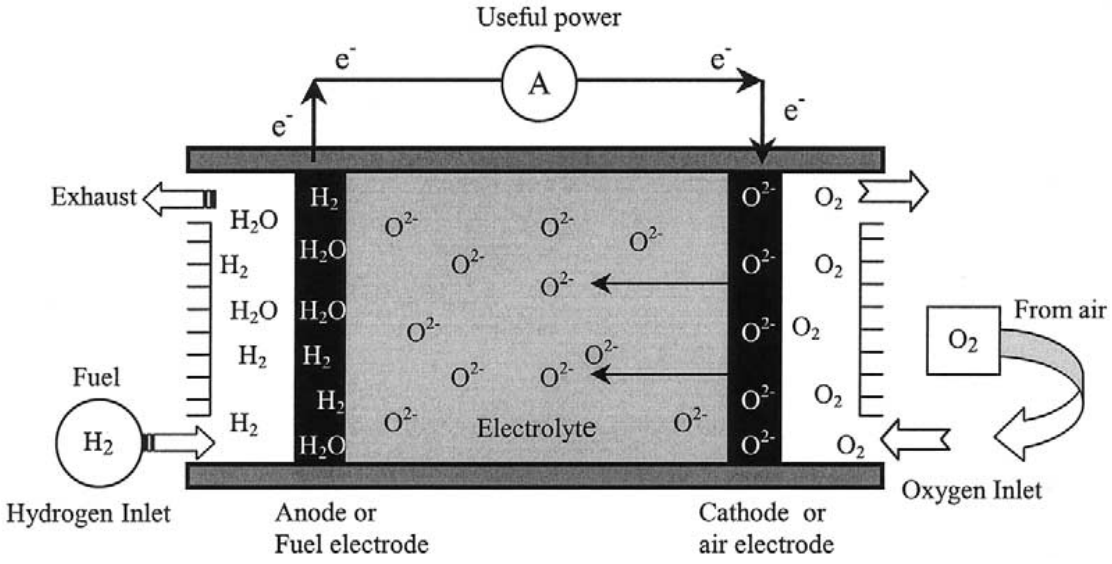

Figure 2 The schematic diagram of the operation in SOFCs based on oxygen ion conductor

Source: Boudghene and Traversa (2002)

SOFCs are constructed with two porous electrodes sandwiched with a dense electrolyte. When the air (O_2) flowing along the cathode to contact the cathode/electrolyte interface, it catalytically acquires four electrons from the cathode and splits into two oxygen ions. The oxygen ions diffuse into the electrolyte material and migrate to the anode to encounter the fuel (H_2). At the anode/electrolyte interface, the oxygen ion and H_2 react catalytically to provide water, carbon dioxide, heat, and most importantly electrons. The electrons transport though the anode to the external

circuit and back to the cathode, providing a source of powerful electrical energy in an external circuit. All the reaction are shown as follows.

Cathode:	$O_2 + 4e^- = 2O^{2-}$
Anode:	$H_2 + O^{2-} = H_2O + 2e^-$
Overall reaction:	$2H_2 + O_2 = 2H_2O$

2.1 Cell Components and Requirements (Singhal, 2000)

2.1.1 Anode

The anode layer must be very porous to allow the fuel to flow towards the electrolyte. The most common material is a cermet made up of nickel mixed with the ceramic material used for the electrolyte (YSZ, Yttria-stabilized zirconia. The anode is commonly the thickest and strongest layer in each individual cell, because it has the smallest polarization losses, and is often the layer providing the mechanical support. Electrochemically operation of the anode is to use the oxygen ions diffusing to the electrolyte to oxidize the hydrogen fuel to produce water and electricity.

2.1.2 Electrolyte

The electrolyte is a dense layer of oxygen ion conducting ceramic to conduct the oxide ions between the anode and cathode. Its electronic conductivity must be low to prevent losses from leakage currents. The high operating temperatures of SOFCs provide the sufficient kinetics of oxygen ion transport for good performance. However, the ionic transport resistances affecting the performance of SOFCs are appeared during the temperature operated at 600°C. Yttria-stabilized zirconia (YSZ) is the most common electrolyte, while other materials as doped Bismuth, doped perovskite, and doped ceria are developed.

2.1.3 Cathode

The cathode is a thin porous layer where the oxygen reduction takes place. Cathode material must be minimum electronically conductive. Currently, lanthanum strontium manganite (LSM) is chosen for commercial because of its compatibility with doped zirconia electrolyte. Mechanically, it has similar coefficient of thermal expansion to YSZ and thus limits stresses built up from CTE mismatch. Although, LSM works at high temperatures, its performance quickly drops at temperature <800°C. In order to increase the cathode performance, composite cathodes consisting of LSM-YSZ have been developed. In addition, mixed ionic/electronic conducting (MIEC) ceramics, such as the perovskite LSCF, have been researched.

2.1.4 Interconnect

The interconnect can be either a metallic or ceramic layer placing between each individual cell. Because the interconnect is exposed to both the oxidizing and reducing sides of the cell at high temperatures, it must be extremely stable. For this reason, ceramics are suitable for using as the interconnect materials. However, the ceramic interconnect materials are very expansive as compared to metals. Nickel- and steel-based alloys promising as lower temperatures (600-800°C) SOFCs are then developed. Nowadays, the most common interconnect materials are doped lanthanum chromites.

3. Doped Ceria Electrolytes

The most important property of a candidate solid electrolyte material is, of course, the ionic conductivity. Conductivity data of a broad range of solid electrolyte are summarized in Figure 3. In this work, the doped ceria electrolyte is considered and reported.

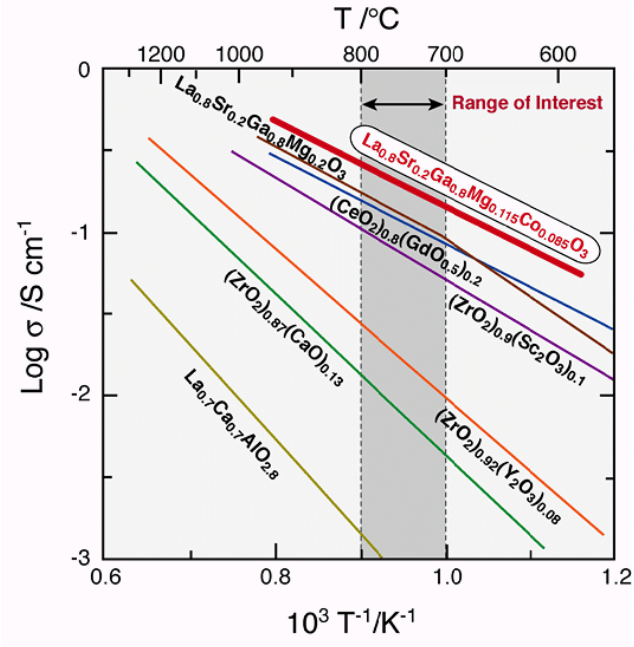

Figure 3 Conductivities of selected solid electrolyte materials as a function of temperature

Cerium(IV) oxide, ceria or cerium oxide (CeO_2), a yellow powder, has a fluorite crystal structure (face centered cubic unit cell with space group *Fm3m*) as shown in Figure 4.

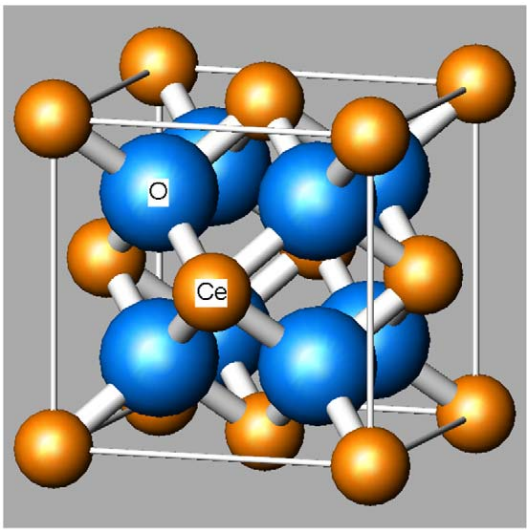

Figure 4 The crystal structure of CeO_2

Source: Haile (2003)

In the doped form, ceria has much attractive for using as an electrolyte material for SOFCs. CeO_2 doped with CaO, Y_2O_3, and various rare earth oxides is an excellent oxygen ion conductor. Doped CeO_2 has been proposed since it shows a higher conductivity and lower conduction activation energy.

The conductivity of doped CeO_2 is influenced by several factors, such as type of dopants, dopant concentration, grain boundary, local structure, microdomain, grain size, impurity, and processing condition.

4. Magnesium Aluminate ($MgAl_2O_4$) from Oxide One Pot Synthesis (OOPS) Process

Laobuthee *et al.* prepared magnesium aluminate ($MgAl_2O_4$) spinel for using as humidity sensors via the OOPS process. The reaction of aluminium hydroxide ($Al(OH)_3$), magnesium oxide (MgO) and triethanolamine (TEA, $N(CH_2CH_2OH)_3$) in ethylene glycol (EG, $HOCH_2CH_2OH$) was carried out to prepare the metal complex or the spinel precursor for $MgAl_2O_4$ (Figure 5).

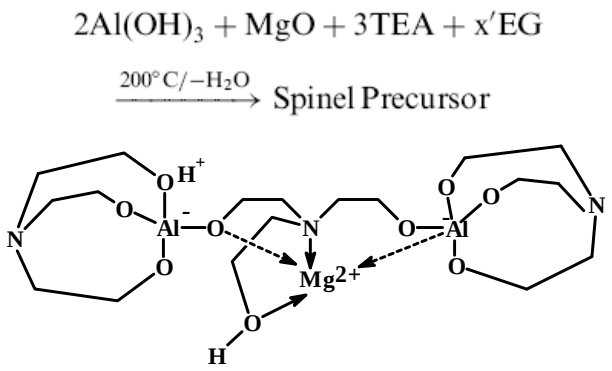

Figure 5 The reaction of OOPS process to prepare magnesium aluminate precursor

The structure of spinel precursor was proposed to be a trimetallic species, consisting of one TEA group per metal center. The spinel precursor was used to prepare $MgAl_2O_4$ powder by calcination process. The obtained $MgAl_2O_4$ exhibited good humidity sensitivity as comparing to that prepared via other methods (Laobuthee *et al.*, 2000).

5. Review of Some Researches

Torren *et al.* (1998) studied the physical and electrical properties of $(CeO_2)_{0.8}(GdO_{0.15})_{0.2}$ powder from different synthesis routes; a modified co-precipitaion reaction, a solid state reaction and a commercial powder from a hydrothermal synthesis route. The modified co-precipitation reaction was carried out by dissolving $Ce(NO_3)_3$ and $Gd(NO_3)_3$ in distilled water and used the oxalic acid (0.05 M) as a precipitant. The pH value was adjusted in the range of 6.7-6.9 by using NH_4OH. The obtained precipitates were calcined at 700°C for 1 h. A solid state method was done by mixing and milling starting oxide powders in a roller-mill and used water-free ethanol as a milling solvent. The starting materials were milled for 24 h, dried at 40°C for 12 h and calcined at either 1200 or 1300°C. A hydrothermal synthesis route from the commercialization was done by co-precipitation of mixed cerium-gadolinium hydroxide gel following with hydrothermal treatment and purification. The ceramic powder was obtained after calcined at 700°C for 1 h. It was found that the powders prepared via solid state technique or co-precipitation had approximately the same particle sizes, but the commercial powder consists of smaller particle size. The results from sintering process showed that the solid state reaction produced very inferior ceramics than those produced via co-precipitation technique, although the particle size ranges were similar. The commercial powder provided a ceramic with a density of 96% theoretical during sintering at 1400°C. The ionic conductivities of pellets at 800°C were found to be 4.5×10^{-2} S/cm and 3.2×10^{-1} S/cm for the powders from solid state reaction and co-precipitation, respectively.

Dikmen *et al.* (2002) prepared $Ce_{1-x}Gd_xO_{2-\delta}$ (x = 0-0.3) solid solution by hydrothermal synthesis method. The procedure was started by dissolving $Ce(NO_3)_3 \cdot 6H_2O$ and $Gd(NO_3)_3 \cdot 6H_2O$ separately in water, mixed and co-precipitated with NH_4OH at pH = 10. The precipitate gels were hydrothermally treated at 260°C for 10 h and quenched to room temperature. The obtained crystallized powders of $Ce_{1-x}Gd_xO_{2-\delta}$ (x = 0-0.3) solid solution has particle size in the range of 41-68 nm. The highly dense ceramic pellets sintered at 1300-1400°C were obtained. The highest

conductivity was found for 0.25 mol% Gd substitution and the activation energy was 0.58 eV. They concluded that gadolinium-doped ceria prepared via hydrothermal synthesis method exhibits the highest conductivity.

Peng and Zhang (2006) synthesized $Ce_{1-x}Gd_XO_{2-\delta}$ (x = 0-0.6) solid solution by nitrate-citrate combustion method (gel-combustion). The stoichiometric ratios of $Ce(NO_3)_3$ and $Gd(NO_3)_3$ solution were mixed. Citric acid was added to the solution. The pH value of the solution was adjusted to 8.0 by adding NH_4OH. The solution becomes a transparent gel at 60-70°C. The gels were then calcined at 500°C to obtain the ceramic powder. The particle size of $Ce_{1-x}Gd_XO_{2-\delta}$ obtained from this synthesis route was 11-28 nm. The powders were then pressed into pellets and sintered at 1300°C for 10 h. The highest conductivity was found for the x = 0.2 Gd substitution ($\sigma_{600°C}$ = 5.26 x 10^{-3} S/cm).

Thangadurai and Kopp (2007) presented a chemical synthesis for preparation of nano-crystalline powders of CeO_2 and Ca-doped CeO_2 at 400°C from $CaCl_2$ and $(NH_4)_2Ce(NO_3)_6$ and oxalic acid. The preparation of Ca-doped ceria by solid state reaction was done to compare with the chemical synthesis method using CeO_2 and $CaCO_3$ as starting materials. The mixtures of CeO_2 and $CaCO_3$ were sintered at 1500°C for 24 h and annealed at 1000-1350°C for 24 h. They found the formation of a single phase fluorite structure of $Ce_{1-x}Ca_xO_{2-x}$ (x = 0-0.2) at 220°C but the XRD patterns were broad and sharp with increasing temperature. By comparing with the solid state reaction, the lattice parameters increases with increasing amount of Ca up to 0.10 mol%. This implied that the Ca-doped CeO_2 was successfully by co-precipitation method.

Jiang-dong *et al.* (2007) synthesized ceria (CeO_2) nanoparticles by pyrolysis method using hydrate cerium propionate as a precursor. The crystalline cerium propionate was converted to ceria by calcining at given temperature for 90 min. The results showed that the calcination temperature affected the physical properties of ceria particles. The higher calcination temperatures, the smaller and denser particles were obtained. The particle size of ceria was in the range of 20-50 nm. In addition, the

specific surface area and the negative value of Zeta potential were decreased with increasing of calcination temperature.

Fuentes and Baker (2008) used the cation complexation for preparing gadolinium-doped ceria solid solution at 0.1 mol% gadolinium substitution from cerium nitrate, gadolinium nitrate, and citric acid. The transparent gel was calcined at 500°C for 1 h to obtain the single powder. The sample has an average crystallite size ~10 nm. The electrical conductivities of pellet samples were studied with two sintering conditions; sintered at 1300°C for 30 h and 1400°C for 8 h. They found that two sintering conditions have no effect on total conductivity but at low temperature, the sintering condition at 1300°C for 30 h gives the highest grain boundary conductivity. In addition, the impedance spectra showed no effect from the etching treatments for total conductivity while grain boundary conductivity decreased.

Santos *et al.* (2008) have been successfully prepared the crystalline ceria (CeO_2) nanoparticles by microwave-hydrothermal method from $(NH_4)_2Ce(NO_3)_6$ and PEG (surfactant). NH_4OH was then added to the solution until the pH 9. The solution was heated up to 130°C for 20 min to obtain CeO_2 powders. The obtained CeO_2 powders were calcined at 500°C for 1, 2 and 4 h. From field-emission scanning electron microscopy, the narrow distribution of ceria particles exhibiting weak agglomeration was found. This method can be used to prepare CeO_2 powders in the short time at low temperature.

MATERIALS AND METHODS

Materials

1. Electrochemical Impedance Spectrometer (EIS, Solartron SI 1260 impedance analyzer)
2. Fourier Transform Infrared Spectrophotometer (FTIR, Perkin Elmer system 2000 FTIR)
3. Electrospray Ionization Mass Spectrometer (ESI-MS, Bruker Esquire mass spectrometer)
4. Thermogravimetric Analyzer (TGA/DSC, Model TGA/DSC 851e, Mettler Toledo)
5. X-ray Diffractrometer (XRD, Bruker D8-Advance X-ray diffractrometer)
6. Scanning Electron Microscope (SEM, XL30 series, Phillips)
7. Surface Area Analyzer (BET, Micromeritics ASAP 2020 surface analyzer)
8. Cold Isostatic Pressing (CIP)
9. Hot Plate Magnetic Stirrer
10. Rotary Evaporator
11. High Temperature Furnace
12. Balance
13. Laboratory Test Sieve
14. Glassware
15. Cerium(III) chloride hepta-hydrate ($CeCl_3 \cdot 7H_2O$, Acros Organics, 99.0% purity)
16. Gadolinium(III) chloride hexa-hydrate ($GdCl_3 \cdot 6H_2O$, Sigma, 99.0%)
17. Samarium(III) chloride hexa-hydrate ($SmCl_3 \cdot 6H_2O$, Acros Organics, 99.0% purity)
18. Triethanolamine (TEA, $N(CH_2CH_2OH)_3$, Carlo Erba, 98% purity)
19. Propan-1-ol ($CH_3CH_2CH_2OH$, Carlo Erba, 99.5% purity)

Methods

1. Preparation and Characterization of Metal Complex

1.1 Preparation of Metal Complex

The cerium complexes of CeO_2 and $Ce_{1-x}Re_xO_{2-\delta}$ (x = 0, 0.10, 0.15 and 0.20, Re = Gd and Sm) powders were prepared via metal complex as follows.

$$CeCl_3 \cdot 7H_2O + (ReCl_3 \cdot 6H_2O) + TEA + \text{propan-1-ol} \longrightarrow \text{Cerium complex}$$

The stoichiometric ratios of $CeCl_3 \cdot 7H_2O$ and $ReCl_3 \cdot 6H_2O$ were mixed in propan-1-ol and added into the round bottom flask. Triethanolamine (TEA) was then added to the solutions in the molar ratio of TEA to metal chloride as 1:1 in order to form complex with rare earth metal. The mixtures were heated to distill-off propan-1-ol and crystalline water until the precipitates occurred. The mixtures were evaporated to remove organic solvent and obtain the white colored powders of cerium complexes.

1.2 Characterization of Metal Complex

1.2.1 Functional Group Analysis

The obtained cerium complexes were characterized by Fourier transform tnfrared spectrophotometer (FTIR, Perkin Elmer system 2000 FTIR). The powder samples were grinded thoroughly with KBr and uniaxially pressed into pellet sample before measurement. All the peaks were recorded in range 4000-400 cm^{-1} with a spectral resolution of 4 cm^{-1} using transparent potassium bromide (KBr) pellet.

1.2.2 Molecular Weight Determination

Electrospray ionization mass spectrometer (ESI-MS, Bruker Esquire mass spectrometer) was employed to determine the molecular weight of obtained

cerium complexes. The cerium complexes were dissolved in methanol used as matrix. The spectra were recorded in positive mode on a micrOTOF instrument. The mass range of samples was set from m/z = 50 to 3000. The scanning time for each sample was 2.4 min.

1.2.3 Thermogravimetric Analysis

The decomposition aspect and weight loss of all the cerium complexes were studied by thermal analysis which carried out with a TGA/DSC analyzer. Samples were loaded in an alumina crucible and heated at the heating rate of 5°C/min under the air. The curves were recorded at the temperature range 50-1500°C.

2. Preparation and Characterization of Ceramic Powders

2.1 Preparation of Ceramic Powders

To obtain the ceramic powders, all the complexes were converted to ceramic powders by calcination process. All the complexes were calcined in alumina crucibles at the temperatures of 600, 800, and 1000°C for 2 h in air. The effects of calcination temperatures were studied by various techniques (XRD, BET, and SEM).

2.2 Characterization of Ceramic Powders

2.2.1 Phase Identification

Calcined powders were studied by X-ray diffraction (XRD) using a Bruker D8-Advance X-ray diffractrometer with CuK_{α} radiation. Diffraction patterns were recorded over a range of 2θ angles from 20 to 90 degree in a step-scanning mode (0.02° steps with a step counting time of 2 s). The crystalline phase was identified from the Joint Committee on Powder Diffraction Standard (JCPDS) file No. 34-0394.

The crystallite size, D_{XRD}, of the calcined powders were estimated using the Scherrer equation;

$$D_{XRD} = 0.9\lambda / \beta\cos\theta \qquad (1)$$

Where λ is the wavelength of the X-ray (1.5406 Å), θ is the scattering angle of the main reflection (111), and β is the corrected peak at full width at full half-maximum (FWHM) intensity.

2.2.2 Surface Area Analyzer

Specific surface area (S_{BET}) measurements were carried out using Brunauer-Emmett-Teller (BET) analysis by nitrogen adsorption isotherms at 77 K using a Micromeritics ASAP 2020 surface analyzer and a value of 0.162 nm^2 for the cross section of the nitrogen molecule. Samples were degassed at 350°C under nitrogen vacuum for 20 h before measurement.

The S_{BET} were translated into the average particle size (D_{BET}) according to the formula;

$$D_{BET} = 6000 / (d_{th} \times S_{BET}) \qquad (2)$$

Where D_{BET} is average particle size (nm), S_{BET} is specific surface area (m^2/g), and d_{th} is the theoretical density of the solid solution oxide (7.215 g/cm^3).

2.2.3 Morphology Observation

The powder morphology was observed by Scanning Electron Microscope (SEM, XL30 series, Phillips) operating at an acceleration voltage of 14 kV and magnification value in 10000x to identify the powder structures. Samples were mounted on alumina stubs using carbon tape and then sputter coated with Au to avoid particle charging.

3. Preparation of and Characterization of Pellet Samples

All the powders were palletized in an uniaxial press by stainless steel die under a pressure of 30 MPa, and subsequently isostatically pressed at 200 MPa by Cold Isostatic Pressure (CIP) at 200 MPa. The resultant pellets were sintered in air at 1500°C for 5 h in order to obtain the maximum density.

3.1 Phase Identification

Phase identification of sintered pellet samples was confirmed by X-ray diffraction (XRD) using a Bruker D8-Advance X-ray diffractrometer with CuK_{α} radiation. Diffraction patterns were recorded over a range of 2θ angles from 20 to 90 degree in a step-scanning mode (0.02° steps with a step counting time of 2 s). The crystalline phase was identified from the Joint Committee on Powder Diffraction Standard (JCPDS) file No. 34-0394.

3.2 Density Measurement

The Achemedes method was used to determine the bulk density of the sintered ceramic pellets. The pellet samples were weighed in dry (in air) and suspension condition (in water). Normally, the pellets were found to have a density above 90% of their theoretically determined density. The dry weight (D), saturated weight (W), suspended weight (S) and density of water (ρ) were measured and used to calculate the bulk density by using the equation as below.

$$\text{Bulk density} = [D / (W-S)]\ \rho \qquad (3)$$

3.3 Morphology of Pellet Samples

The grain size and morphology of the pellet samples were examined using a Phillips XL30 series Scanning Electron Microscope. The pellets were firstly polished with alumina before thermal etching at 1400°C for 2 h in air.

4. Study on Electrical Properties of Pellet Samples

The electrical conductivity of the pellet samples were measured on the sintered ceramic pellets. Gold pastes were painted onto two faces of the pellets to act as electrodes. The pellets were then fired at 800°C for 2 h in air. AC impedance spectra were measured in air with a ZPlot^{TM} (National Instruments) program and a Solartron SI 1260 impedance analyzer. The pellets were placed in an alumina holder using a spring clip arrangement between Pt current collectors and the thermocouple was placed right next to the samples. The samples were heated during the measurement and recorded the spectra from 225 to 700°C in air using a tube furnace with controlled heating rate 3°C/min. The frequency range was measured at 0.1 Hz to 10 MHz.

The resistance (R) of each sample was determined from the intercept on the real axis and the electrical conductivities (σ) were calculated by using equation (4).

$$\sigma = L/RA_e \qquad (4)$$

Where L is thickness and A_e is an area of the electrode.

The activation energy (E_a) and the electrical conductivity of pellet sample were calculated from the plot of ln (σT) vs. 1/T according to the Arrhenius equation (5).

$$\sigma T = A\exp(-E_a/kT) \qquad (5)$$

Where σ is conductivity, A is pre-exponential factor, E_a is activation energy, k is Boltzmann's constant, and T is absolute temperature.

RESULTS AND DISCUSSION

1. Characterization of Metal Complex

The pure cerium complex was firstly prepared from $CeCl_3 \cdot 7H_2O$ and TEA. The reaction was started by dissolving $CeCl_3 \cdot 7H_2O$ in propan-1-ol to obtain the clear solution. TEA was then added to form the cerium complex. After completing the reaction, the homogeneous milky solution of cerium complex was obtained after distillation. After removing the organic solvent, a white powder was obtained.

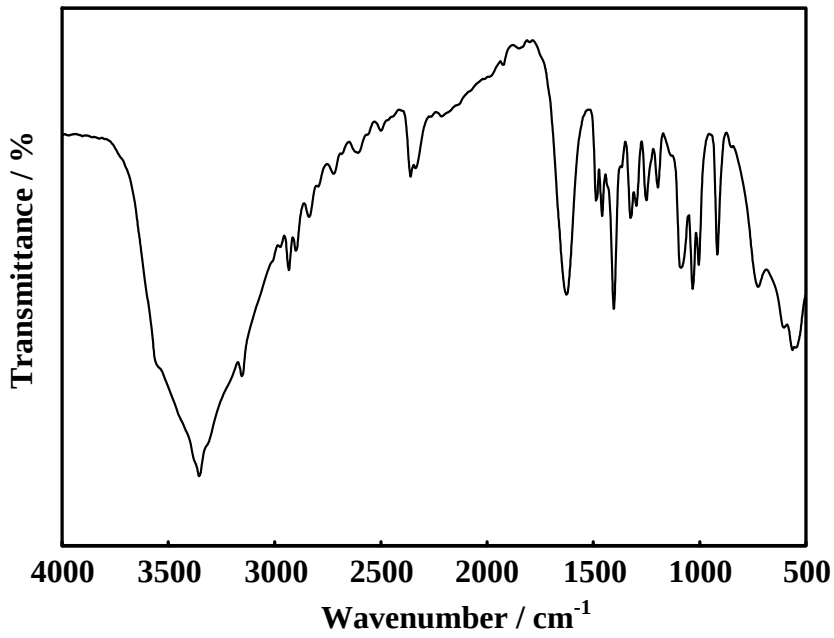

Figure 6 FTIR spectrum of the pure cerium complex

To identify the possible structures of cerium complex, the cerium complex was firstly characterized by FTIR and the spectrum of the pure cerium complex is showed in Figure 6. The broad peak located at 3358 cm^{-1} was assigned to the O-H stretching due to the moisture absorption and/or triethanolamine-residue from the reaction. The C-H stretching bands at 2928 and 2890 cm^{-1} were assigned to $-CH_2-$ group. The C-H bending bands were shown in the region of 1450-1200 cm^{-1}. The band at 1629 cm^{-1} was attributed to O-H overtone. Moreover, the resonance at 1079

cm^{-1} was ascribed to the Ce-O-C stretching vibration, while the band at 564 cm^{-1} was assigned to the Ce-O stretching.

The product structures were then identified by ESI-MS. The MS spectrum of the pure cerium complex is shown in Figure 7. It indicates that there are two intense peaks at m/z = 286 and 322 corresponding to [Ce(TEA)] and [Ce(TEA)Cl] complexes, respectively.

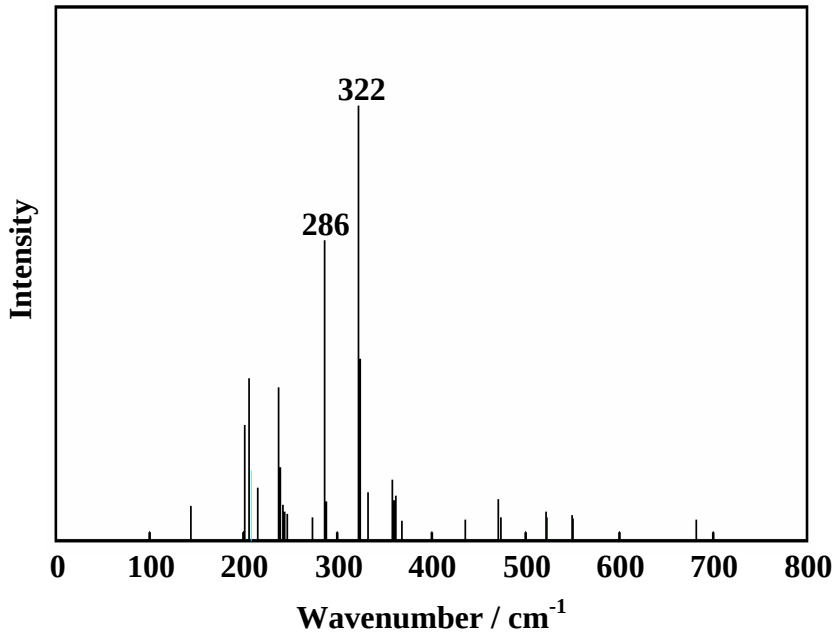

Figure 7 Mass spectrum of the pure cerium complex

Based on the results from FTIR and ESI-MS, two possible structures of cerium complexes (Figure 8) can be proposed as four coordinated cerium ion binding to TEA molecule (Structure I) and five coordinated cerium ion with TEA and Cl^- ligands (Structure II).

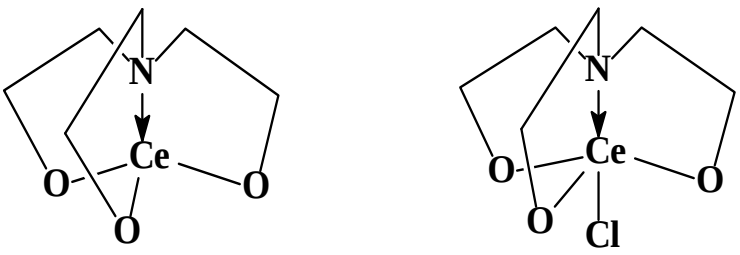

Figure 8 The two possible structures of cerium complexes

The cerium complexes of $Ce_{1-x}Gd_xO_{2-\delta}$ and $Ce_{1-x}Sm_xO_{2-\delta}$ (x = 0.10, 0.15 and 0.20) were consequently prepared via metal complex method. The stoichiometric ratios of $CeCl_3 \cdot 7H_2O$ and $ReCl_3 \cdot 6H_2O$ (Re = Gd, Sm) were dissolved in propan-1-ol. TEA was then added to the mixture solution. After completing the reaction, the homogeneous milky solution occurred and the white powders of complexes were obtained after eliminating the organic solvent.

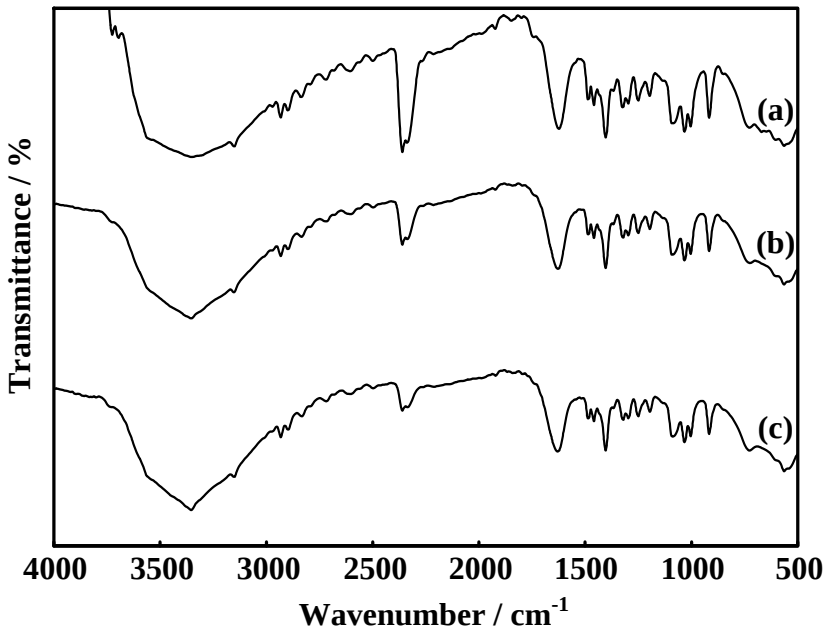

Figure 9 FTIR spectra of cerium complexes doped with (a) 0.10, (b) 0.15, and (d) 0.20 mol% Gd

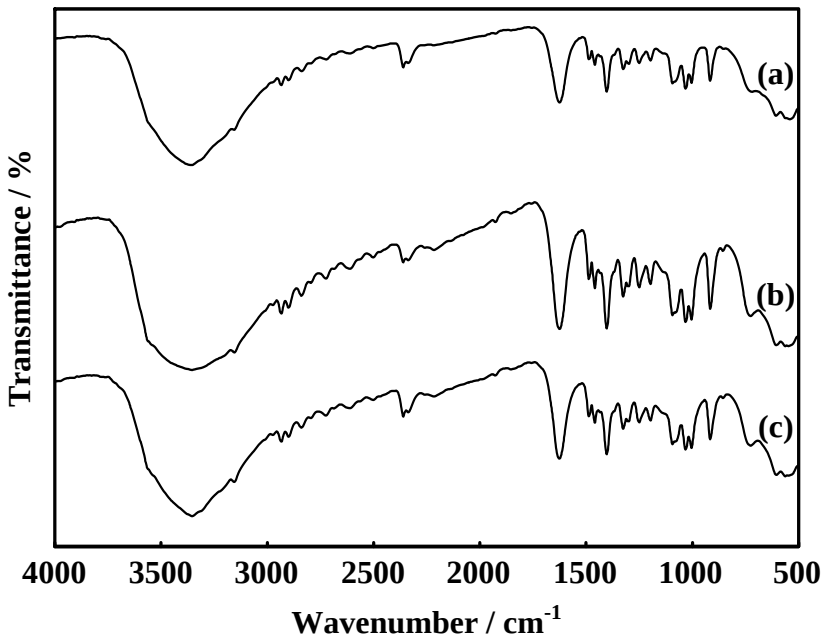

Figure 10 FTIR spectra of cerium complexes doped with (a) 0.10, (b) 0.15, and (d) 0.20 mol% Sm

The doped cerium complexes were characterized by FTIR. The FTIR spectra of the doped cerium complexes are shown in Figures 9 and 10. The doped cerium complexes show the FTIR peaks (Figures 9 and 10) similar to the pure cerium complex (Figure 6). The bands located at 3358 and 1631 cm^{-1} were assigned to the O-H stretching and O-H overtone, respectively. These bands might be due to the water adsorption of products. The peaks at 2928 and 2890 cm^{-1} were attributed to the C-H stretching bands, while the bands at 1450-1200 cm^{-1} are C-H bending bands for $-CH_2-$ group. The peak at 1080 cm^{-1} was ascribed to the Ce-O-C or Gd-O-C stretching vibration for gadolinium doping, and Sm-O-C for samarium doping. In addition, the bands at 564 cm^{-1} was attributed to the Ce-O or Gd-O for gadolinium doping, and Sm-O for samarium doping.

The mass spectra of doped cerium complexes cannot be shown due to the occurrence of the too complicated peaks which generated from the various types of complexes. All the peaks in mass spectra might be the complexes peaks and fragmentation from the complexes.

All the complexes were converted to ceramic powders by calcination process. The appropriate temperature for calcination and weight loss phenomena of complexes were studied by TGA/DSC. The TGA/DSC thermograms of pure cerium complex are comparatively shown in Figure 11. It was found that there are three regions of weight loss. The first weight occurring before 160°C resulted from water evaporation and the removal of organic solvent. The second weight loss happened in temperature ranging 265 to 484°C, a large weight loss in TGA curve and a strong exothermic peak in DSC curve at 337°C involved the decomposition of the organic ligands and generated a char as product. The last gradually weight loss occurred at 485 to 600°C due to the decomposition of organic and/or carbon-residue. After 600°C, the TGA thermogram of pure cerium complex showed no weight loss occurred after 600°C; the appropriate temperature for calcining complexes into ceramic powders might be therefore started at 600°C.

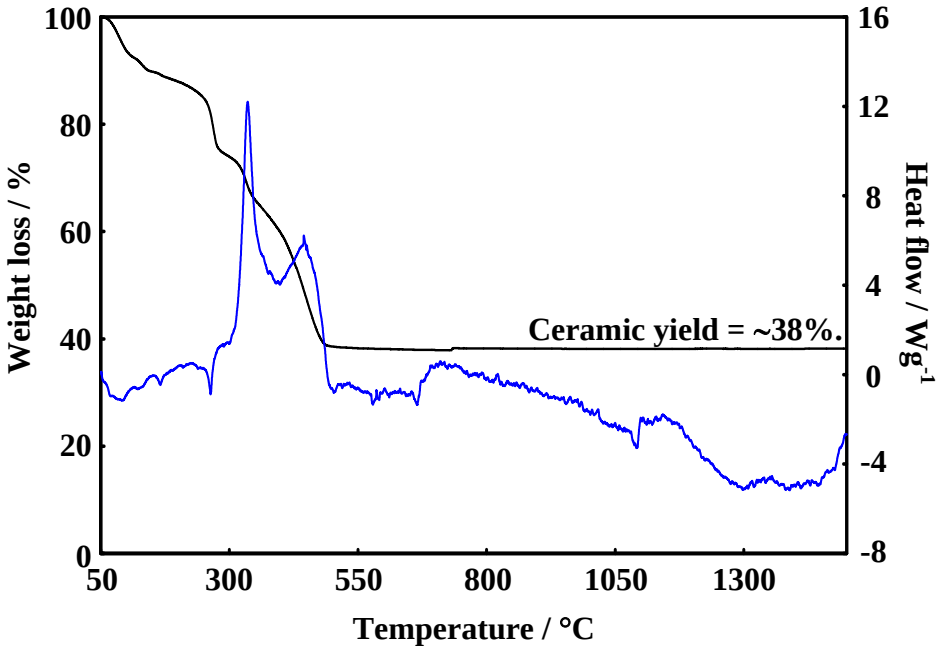

Figure 11 TGA/DSC thermogram of pure cerium complex

In addition, the thermal weight loss of doped cerium complexes shows TGA/DSC thermograms similar to the pure cerium complex. Figures 12 and 13 show

TGA/DSC thermograms of 10% Gd-doped cerium complex and 10% Sm-doped cerium complex, respectively.

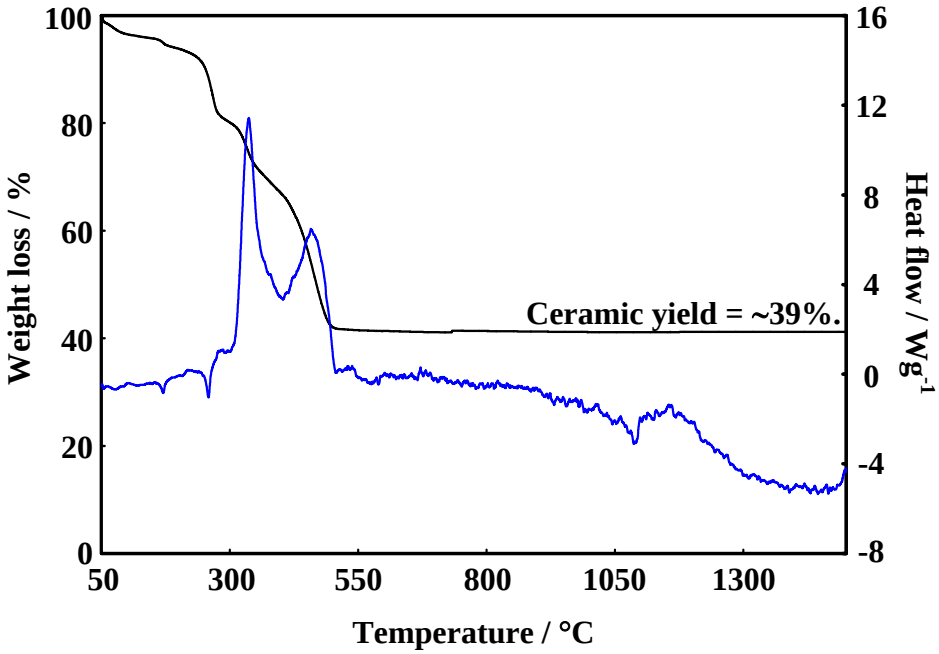

Figure 12 TGA/DSC thermogram of 10% Gd-doped cerium complex

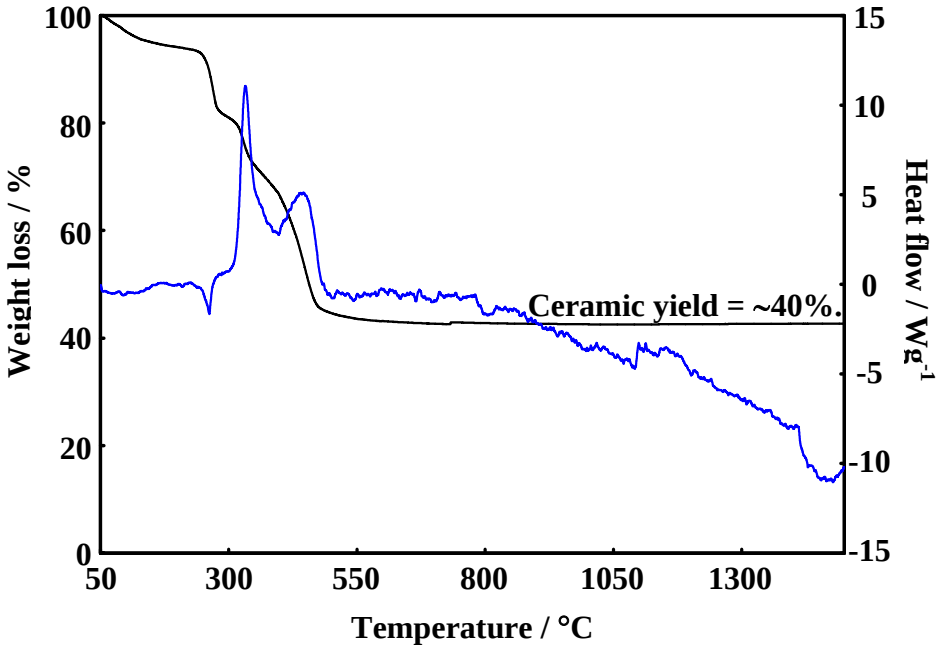

Figure 13 TGA/DSC thermogram of 10% Sm-doped cerium complex

2. Characterization of $Ce_{1-x}Re_xO_{2-\delta}$ Ceramic Powders

To study the effects of calcination temperatures, all complexes were calcined at 600, 800 and 1000°C for 2 h in air. After completing calcination, the light yellowish colored powders of CeO_2, $Ce_{1-x}Gd_xO_{2-\delta}$, and $Ce_{1-x}Sm_xO_{2-\delta}$ ceramic powders were obtained.

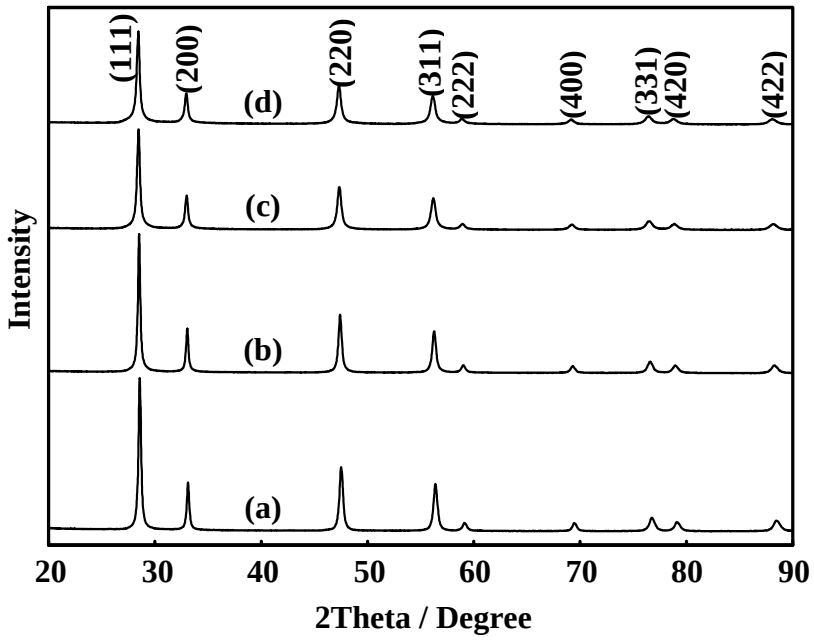

Figure 14 XRD patterns of $Ce_{1-x}Gd_xO_{2-\delta}$ powders; (a) x = 0, (b) x = 0.10, (c) x = 0.15, and (d) x = 0.20, calcined at 600°C for 2 h in air

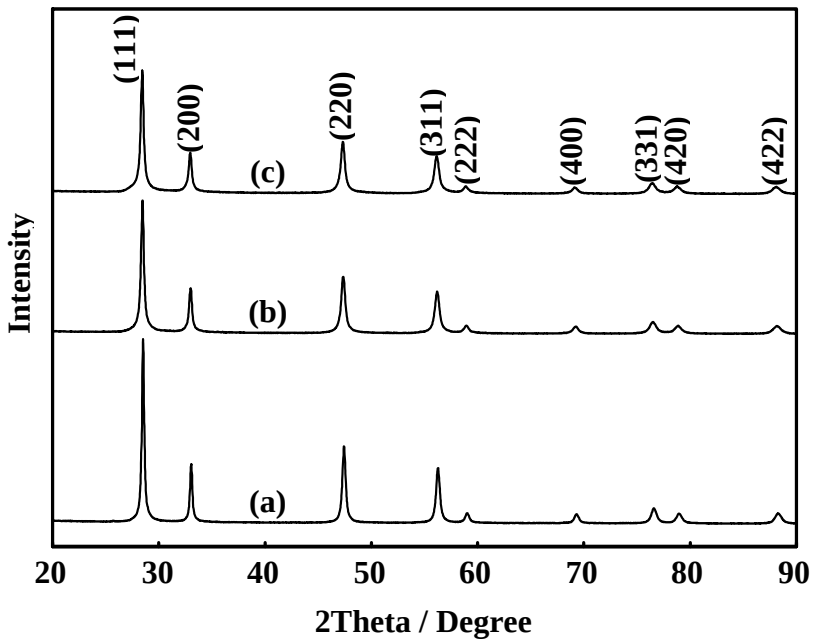

Figure 15 XRD patterns of $Ce_{1-x}Sm_xO_{2-\delta}$ powders; (a) x = 0.10, (b) x = 0.15, and (c) x = 0.20, calcined at 600°C for 2 h in air

All the ceramic powders were identified by XRD technique. Figures 14 and 15 are the X-ray diffraction patterns of $Ce_{1-x}Gd_xO_{2-\delta}$, and $Ce_{1-x}Sm_xO_{2-\delta}$ powders, respectively. It indicated that all compositions of $Ce_{1-x}Gd_xO_{2-\delta}$, and $Ce_{1-x}Sm_xO_{2-\delta}$ are single phase with a cubic fluorite structure (space group *Fm3m*). The characteristic peaks corresponding to (111), (200), (220), (311), (222), (400), (331), (420), and (422) planes which are located at 2θ are 28.535, 33.080, 47.495, 56.348, 59.102, 69.427, 76.710, 79.073, and 88.447 degree, respectively. All the diffraction patterns are identical to that of the original substance of pure CeO_2 (JCPDS No. 34-0394). This implied that the substitution of gadolinium or samarium ion into cerium ion lattice site in ceria structure, consequently, no phase change was observed in the CeO_2 crystal defect. However, it was found that the crystallinity of powders was decreased with the increase of amount of dopants.

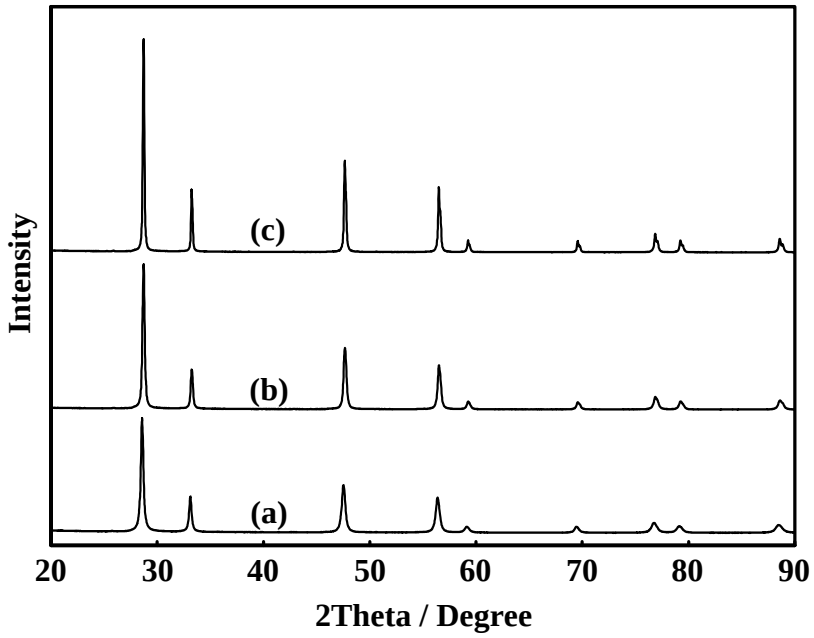

Figure 16 XRD patterns of CeO_2 powders calcined at (a) 600°C, (b) 800°C, and (c) 1000°C for 2 h in air

Figures 16, 17 and 18 show the XRD patterns of CeO_2, $Ce_{0.90}Gd_{0.10}O_{2-\delta}$, and $Ce_{0.90}Sm_{0.10}O_{2-\delta}$ powders calcined at 600, 800, and 1000°C for 2 h in air, respectively. It was found that all compositions have no phase transition occurred from 600 to 1000°C. In addition, all the peaks become stronger and sharper with increasing the temperature. In agreement with the TGA/DSC results, the purity phase of the calcined powders obtained was started at 600°C. Similar XRD patterns to CeO_2 were recorded for ceria doped with 0.15 and 0.20 mol% for both Gd and Sm substitutions.

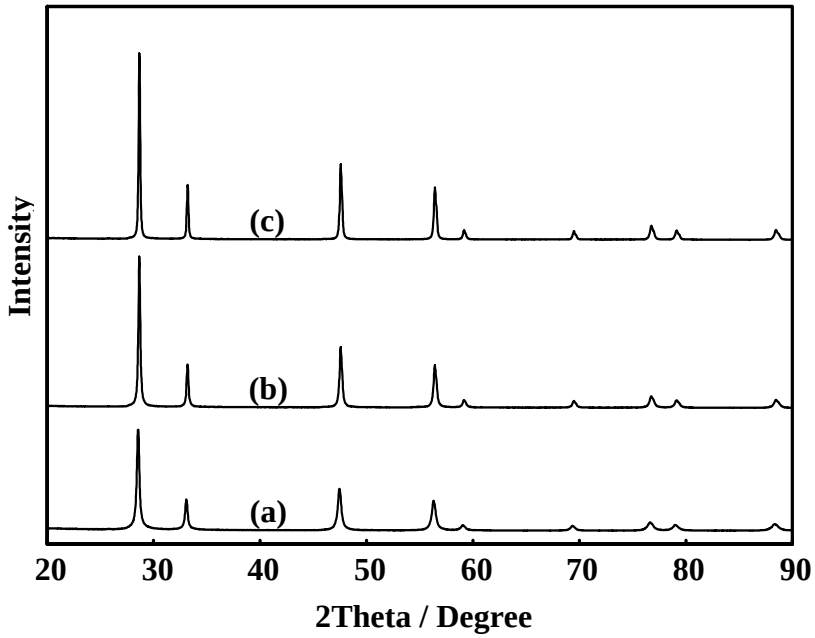

Figure 17 XRD patterns of $Ce_{0.90}Gd_{0.10}O_{2-\delta}$ powders calcined at (a) 600°C, (b) 800°C, and (c) 1000°C for 2 h in air

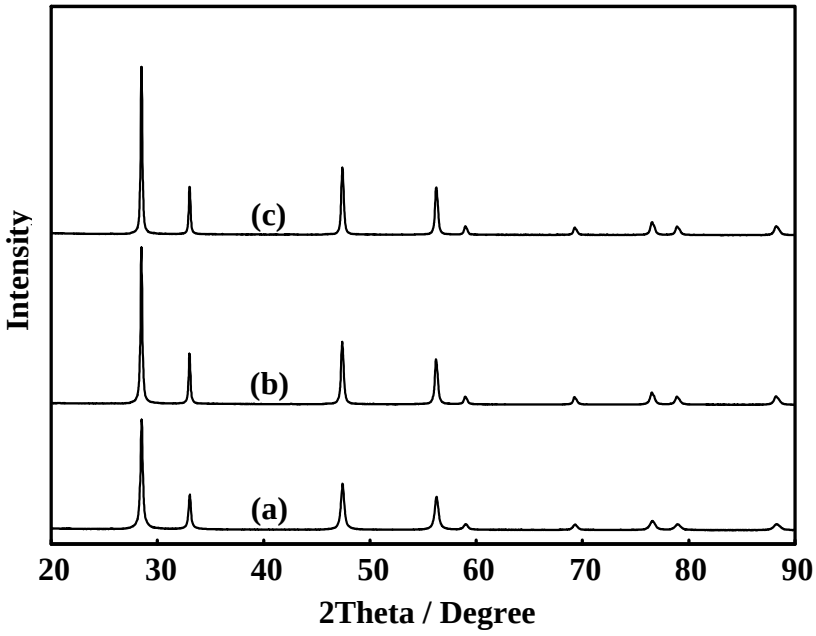

Figure 18 XRD patterns of $Ce_{0.90}Sm_{0.10}O_{2-\delta}$ powders calcined at (a) 600°C, (b) 800°C, and (c) 1000°C for 2 h in air

The crystallite size (D_{XRD}), specific surface area (S_{BET}), and average particle size (D_{BET}) of CeO_2, $Ce_{1-x}Gd_xO_{2-\delta}$ and $Ce_{1-x}Sm_xO_{2-\delta}$ powders calcined at various temperatures for 2 h in air are presented in Tables 2 and 3, respectively. It was found that the crystallite sizes of all the powders as calculated from Scherrer equation are in nanometer unit. Due to the growth of the crystals at high temperature, the crystallite size increases with calcination temperatures increased in agreement with XRD results. Moreover, with the calcination temperatures, the specific surface area (S_{BET}) trend to increase while the average particle size (D_{BET}) decreased.

Table 2 The crystallite size (D_{XRD}), specific surface area (S_{BET}), and average particle size (D_{BET}) of $Ce_{1-x}Gd_xO_{2-\delta}$ (x = 0, 0.10, 0.15, and 0.20) powders calcined at various temperatures for 2 h in air

x	Calcination Temperatures (°C)	Crystallite Size, D_{XRD} (nm)	Specific Surface Area, S_{BET} (m^2/g)	Average Particle Size, D_{BET} (nm)
0	600	32.36	31.31	26.06
	800	36.70	20.98	39.66
	1000	63.23	8.3	100.25
0.10	600	34.25	44.61	18.65
	800	47.65	22.75	36.57
	1000	59.45	7.85	106.00
0.15	600	35.39	46.55	17.88
	800	41.26	28.28	29.42
	1000	47.14	12.73	65.36
0.20	600	29.16	45.34	18.35
	800	30.16	30.92	26.91
	1000	45.46	12.00	69.34

Table 3 The crystallite size (D_{XRD}), specific surface area (S_{BET}), and average particle size (D_{BET}) of $Ce_{1-x}Sm_xO_{2-\delta}$ (x = 0.10, 0.15, and 0.20) powders calcined at various temperatures for 2 h in air

x	Calcination Temperatures (°C)	Crystallite Size, D_{XRD} (nm)	Specific Surface Area, S_{BET} (m^2/g)	Average Particle Size, D_{BET} (nm)
0.10	600	48.51	41.44	20.06
	800	52.14	24.18	34.39
	1000	54.85	14.71	56.53
0.15	600	32.66	51.71	16.08
	800	39.35	30.03	27.69
	1000	43.26	17.50	47.52
0.20	600	36.81	41.25	20.16
	800	41.82	26.67	31.18
	1000	48.69	17.17	48.43

The ceramic powders were further characterized by SEM. Figures 19, 20, and 21 show the SEM micrographs at various calcination temperatures of CeO_2, $Ce_{0.90}Gd_{0.10}O_{2-\delta}$, and $Ce_{0.90}Sm_{0.10}O_{2-\delta}$ powders, respectively. The SEM micrographs showed that calcination temperature affected the microstructure of the powders. All the obtained powders were irregularly shaped with blocky particles possibly because the agglomeration generated with increasing calcination temperatures. In addition, the similar results were observed with 0.15 and 0.20 mol% for both Gd and Sm substitutions.

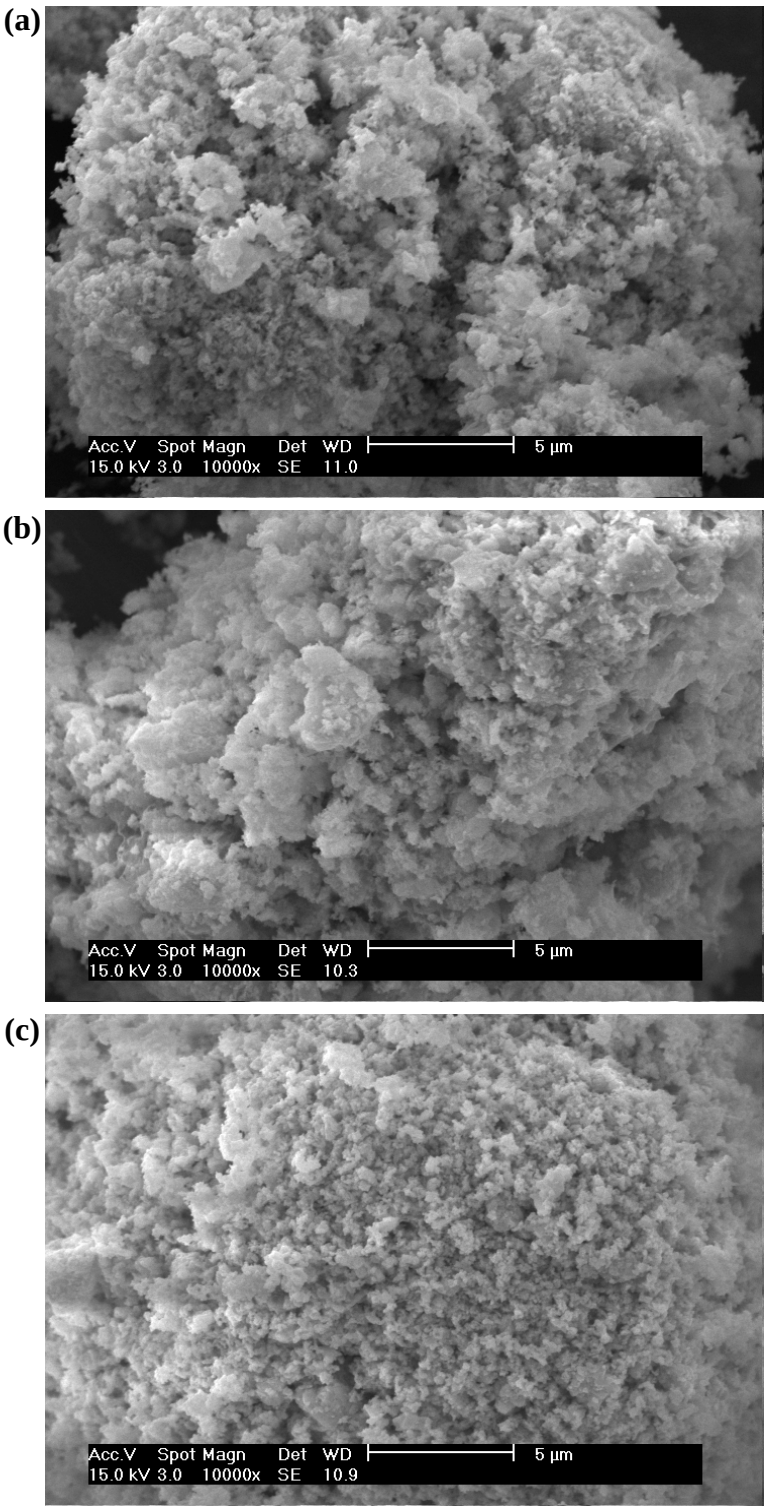

Figure 19 SEM micrographs of CeO_2 powders calcined at (a) 600°C, (b) 800°C, and (c) 1000°C for 2 h in air

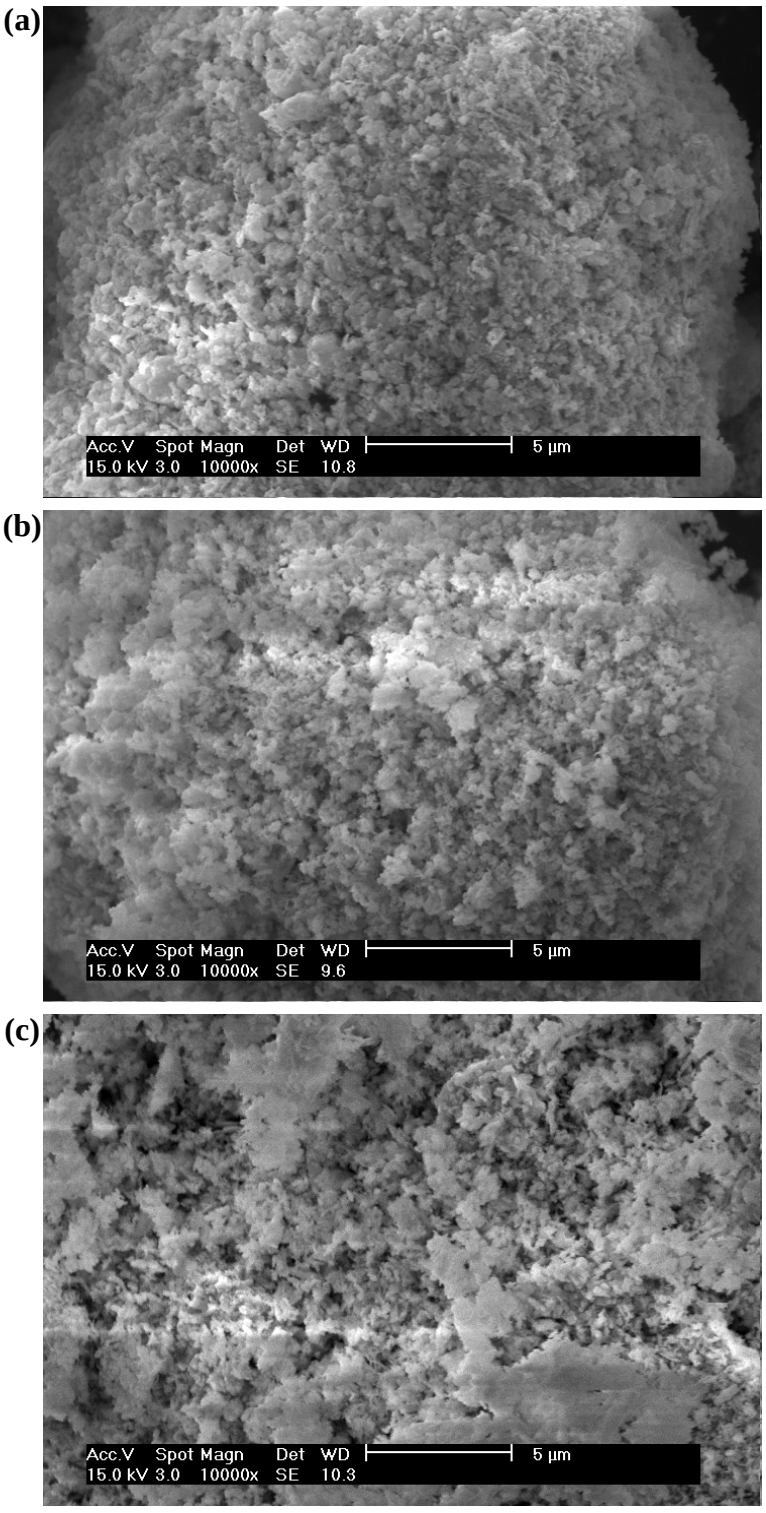

Figure 20 SEM micrographs of $Ce_{0.90}Gd_{0.10}O_{2-\delta}$ powders calcined at (a) 600°C, (b) 800°C, and (c) 1000°C for 2 h in air

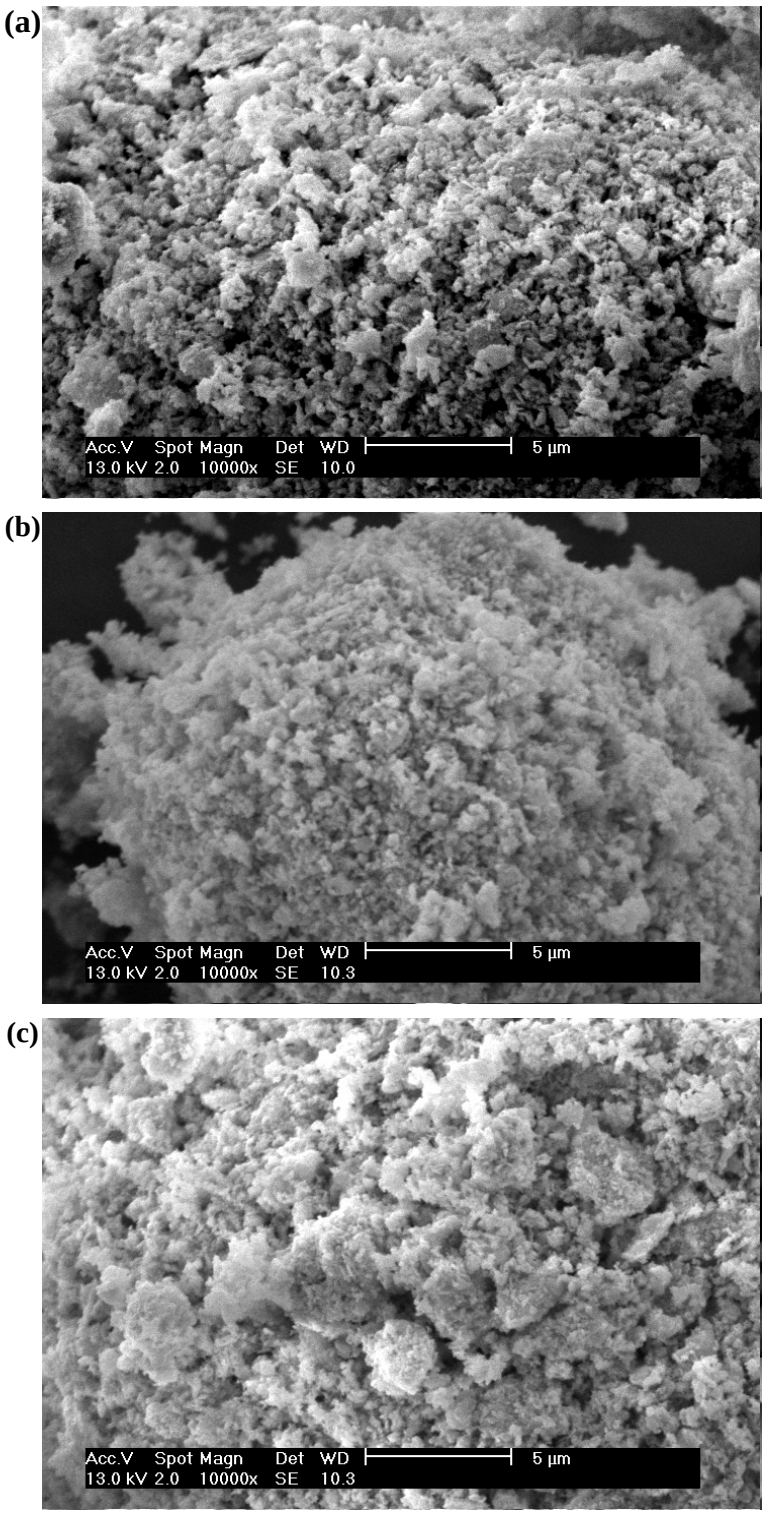

Figure 21 SEM micrographs of $Ce_{0.90}Sm_{0.10}O_{2-\delta}$ powders calcined at (a) 600°C, (b) 800°C, and (c) 1000°C for 2 h in air

3. Characterization of Pellet Samples

To measure the electrical properties of the samples, the ceramic powders were converted to pellet samples by Cold Isostatic Pressing (CIP) and sintered to obtain the maximum density.

The phase identification of all the pellet samples was confirmed by XRD technique. Figures 22 and 23 show XRD patterns of $Ce_{1-x}Gd_xO_{2-x}$ and $Ce_{1-x}Sm_xO_{2-x}$ pellet samples, respectively. It can be seen that XRD patterns of all the pellet samples are similar to CeO_2, $Ce_{1-x}Gd_xO_{2-x}$ and $Ce_{1-x}Sm_xO_{2-x}$ powders (fluorite-typed structure) matched to JCPDS No. 34-0394. This may suggest that there is no phase transition occurred after the compression of ceramic powders into pellet samples. Moreover, the sintering temperature (at 1500°C for 5 h in air) is not affected the crystal structure of pellet samples.

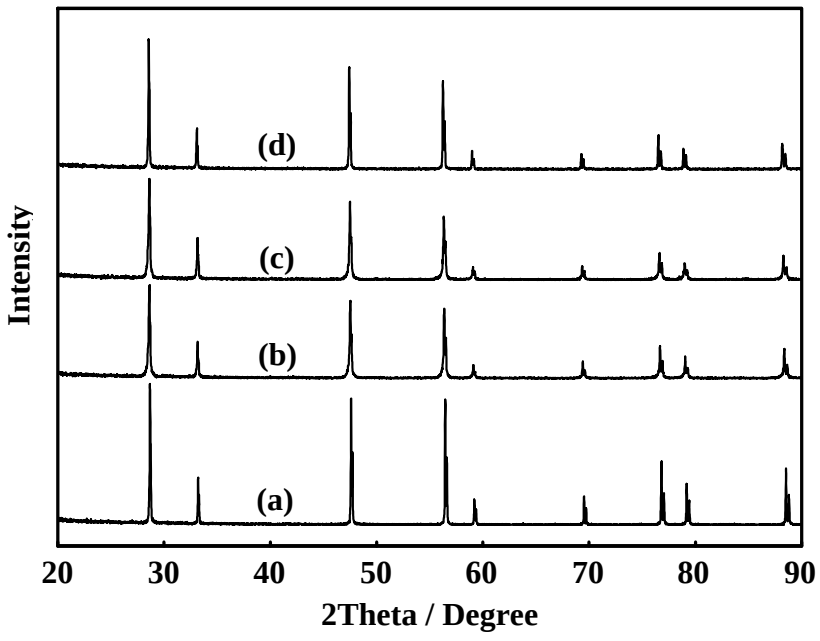

Figure 22 XRD patterns of $Ce_{1-x}Gd_xO_{2-\delta}$ pellets; (a) x = 0, (b) x = 0.10, (c) x = 0.15, and (d) x = 0.20, sintered at 1500°C for 5 h in air

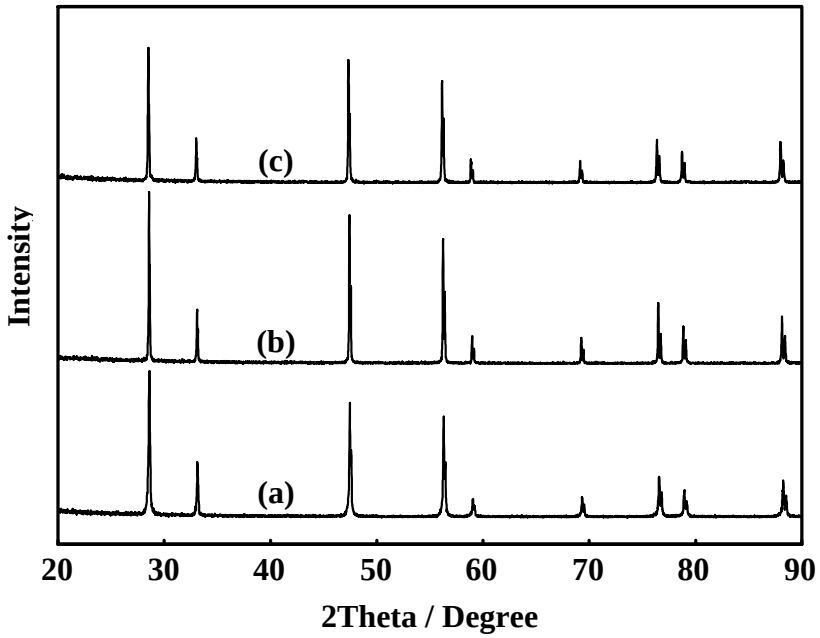

Figure 23 XRD patterns of $Ce_{1-x}Sm_xO_{2-\delta}$ pellets; (a) x = 0.10, (b) x = 0.15, and (c) x = 0.20 sintered at 1500°C for 5 h in air

The bulk densities of pellet samples were determined by Achemedes method. The theoretical densities of the pellets sintered at 1500°C for 5 h in air are listed in Tables 4 and 5. The results showed that the pellets were found to have densities above 90% of their theoretical densities.

Table 4 Theoretical densities of $Ce_{1-x}Gd_xO_{2-\delta}$ pellets sintered at 1500°C for 2 h in air

x	Theoretical density (%)
0	90.11
0.10	92.83
0.15	94.68
0.20	94.20

Table 5 Theoretical densities of $Ce_{1-x}Sm_xO_{2-\delta}$ pellets sintered at 1500°C for 2 h in air

x	Theoretical density (%)
0.10	95.06
0.15	93.93
0.20	94.25

Scanning electron micrographs of $Ce_{1-x}Gd_xO_{2-\delta}$ and $Ce_{1-x}Sm_xO_{2-\delta}$ pellets are illustrated in Figures 24 and 25, respectively.

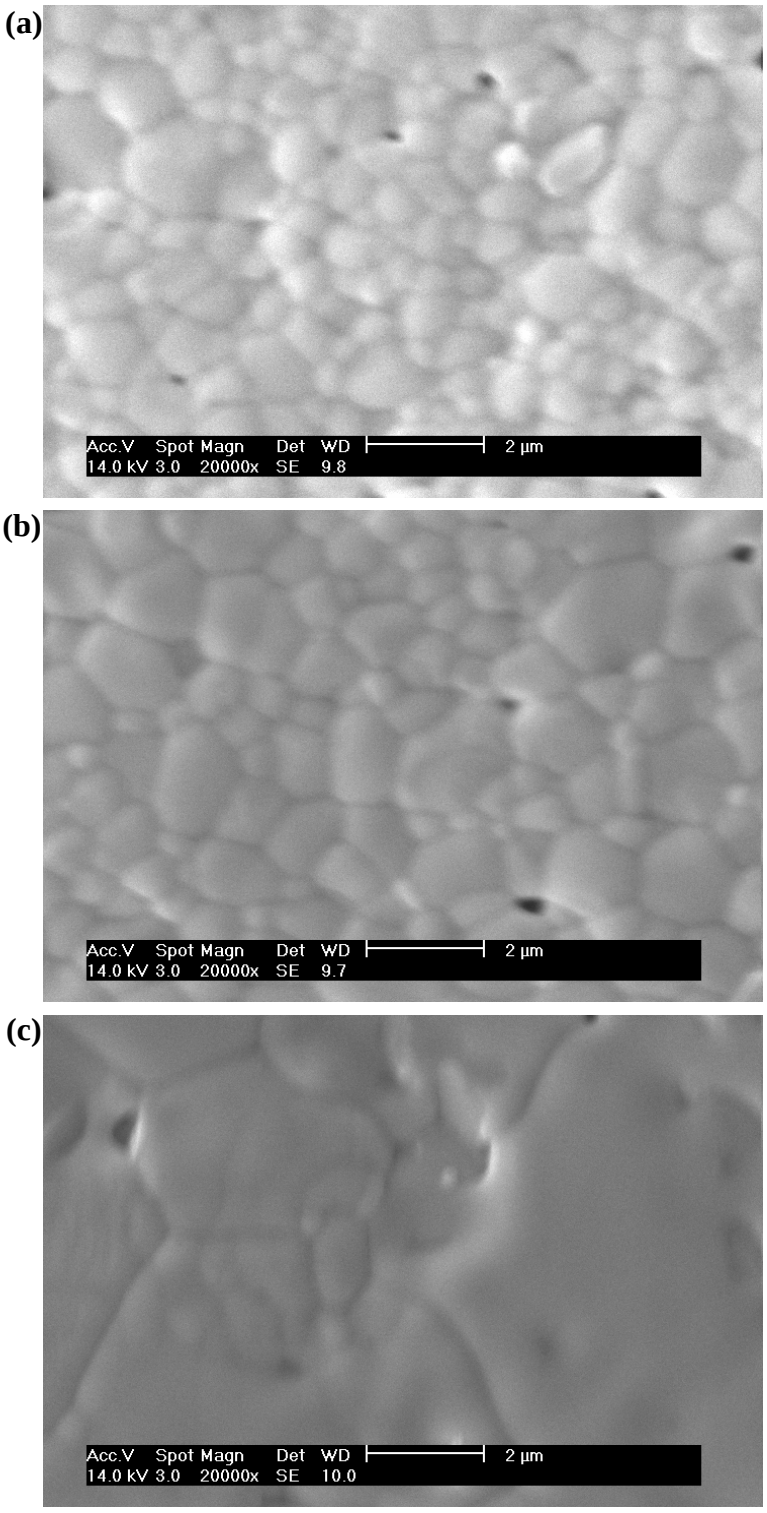

Figure 24 SEM micrographs of $Ce_{1-x}Gd_xO_{2-\delta}$ pellets sintered at 1500°C for 5 h in air and thermal etched at 1400°C for 2 h in air where (a) x = 0.10, (b) x = 0.15, and (c) x = 0.20.

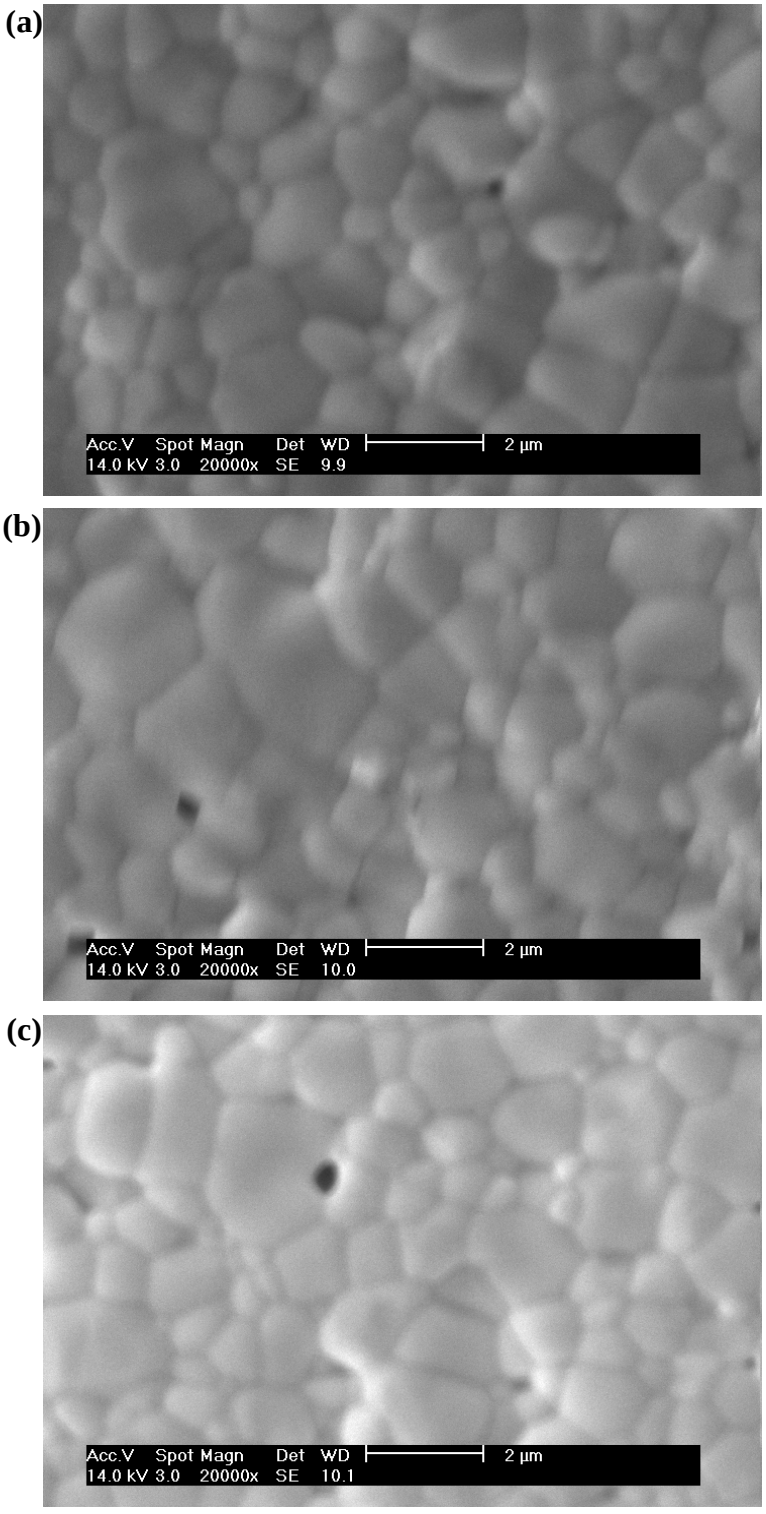

Figure 25 SEM micrographs of $Ce_{1-x}Sm_xO_{2-\delta}$ pellets sintered at 1500°C for 5 h in air and thermal etched at 1400°C for 2 h in air where (a) x = 0.10, (b) x = 0.15, and (c) x = 0.20.

From SEM micrographs of $Ce_{1-x}Gd_xO_{2-\delta}$ pellets, it was found that the grain size of CeO_2 increases with increasing the amount of Gd (Figure 24). In addition, $Ce_{0.85}Gd_{0.15}O_{2-\delta}$ pellet shows the narrow grain size distribution more than $Ce_{0.90}Gd_{0.10}O_{2-\delta}$ and $Ce_{0.80}Gd_{0.20}O_{2-\delta}$ corresponding to the contribution of grain conductivity affecting the total conductivity of $Ce_{0.85}Gd_{0.15}O_{2-\delta}$. Figure 25 shows SEM micrographs of $Ce_{1-x}Sm_xO_{2-\delta}$ pellets. All the pellets (Figure 25a-c) have the same grain size distribution.

4. Ionic Conductivity of $Ce_{1-x}Re_xO_{2-\delta}$ Pellet Samples

The impedance is a well-developed tool to separate out the bulk and grain boundary contribution to the total conductivity. The impedance spectrum is usually represented as negative of imaginary component of impedance (-Z'') versus real component of impedance (Z'), and referred as Nyquist plot. The plot, typically, composed of three semicircles. Each semicircle represents a district process that time constant is sufficiently separated from the others over the range of measurement frequencies. The semicircles at higher and lower frequencies represent bulk and electrode process, respectively, while that at intermediate frequencies represents grain boundary contribution. At higher temperatures, the time constants associated with the bulk and grain boundary impedances are much lower than those associated with the electrode interface. As a result, semicircles due to bulk and grain boundary disappear at higher temperatures, and only a single semicircle due to electrode interfacial processes can be observed.

In general, a pure CeO_2 shows very low ionic conductivity. In this work, we, therefore, reported only the ionic conductivity of doped CeO_2. It is well known that doped CeO_2 behaves as a pure ionic conductor in air with negligible electronic conductivity. Figures 26 and 27 show the typical impedance spectra at various temperatures of $Ce_{0.85}Gd_{0.15}O_{2-\delta}$ and $Ce_{0.9}Sm_{0.10}O_{2-\delta}$ pellets, respectively. The spectra show that three well-defined semicircular arcs were observed in the complex

impedance plane which matched to the theories. Similar spectra were observed for other compositions.

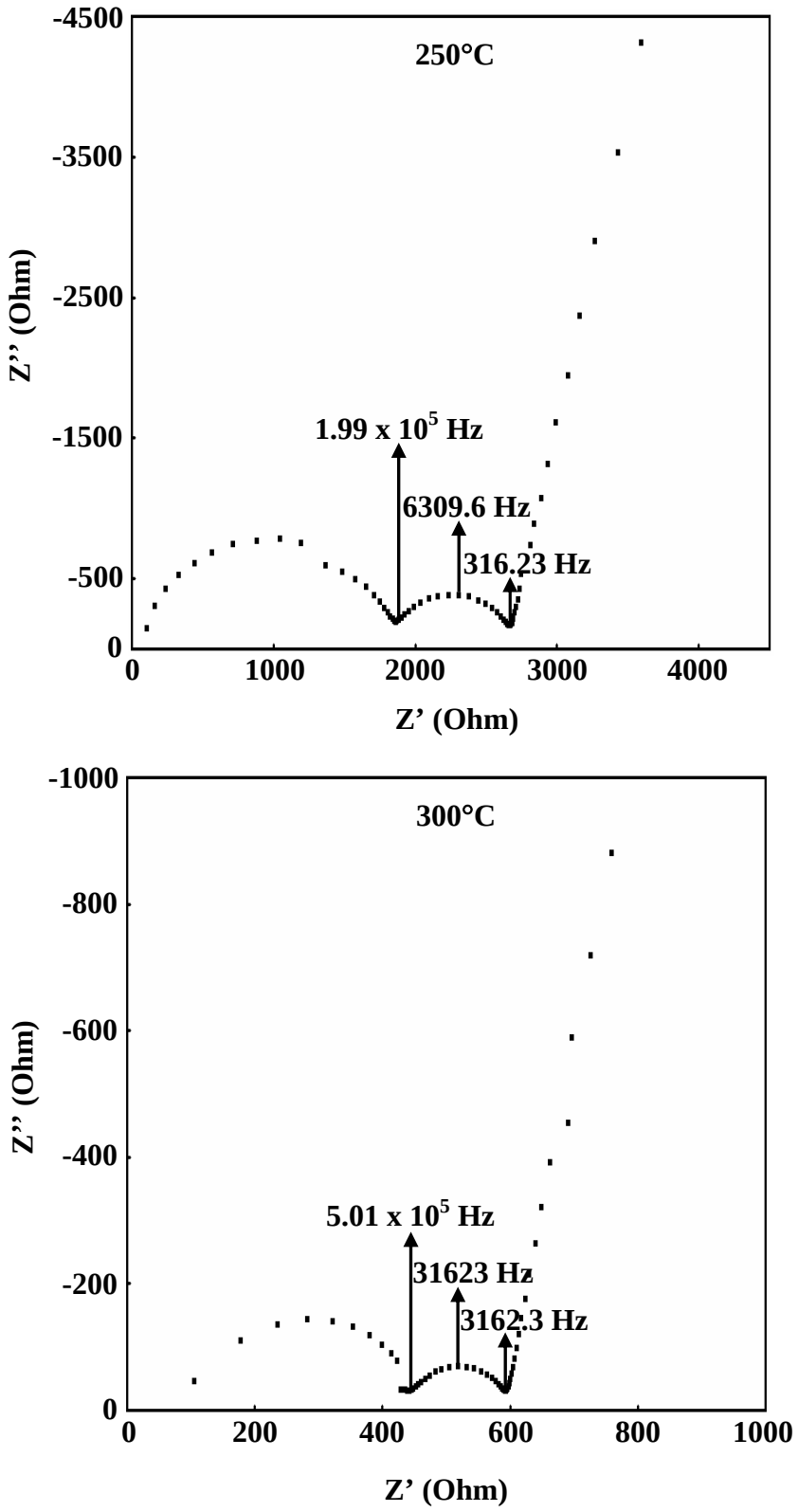

Figure 26 Impedance spectra of $Ce_{0.85}Gd_{0.15}O_{2-\delta}$ pellet which calcined at 600°C for 2 h in air and sintered at 1500°C for 5 h in air

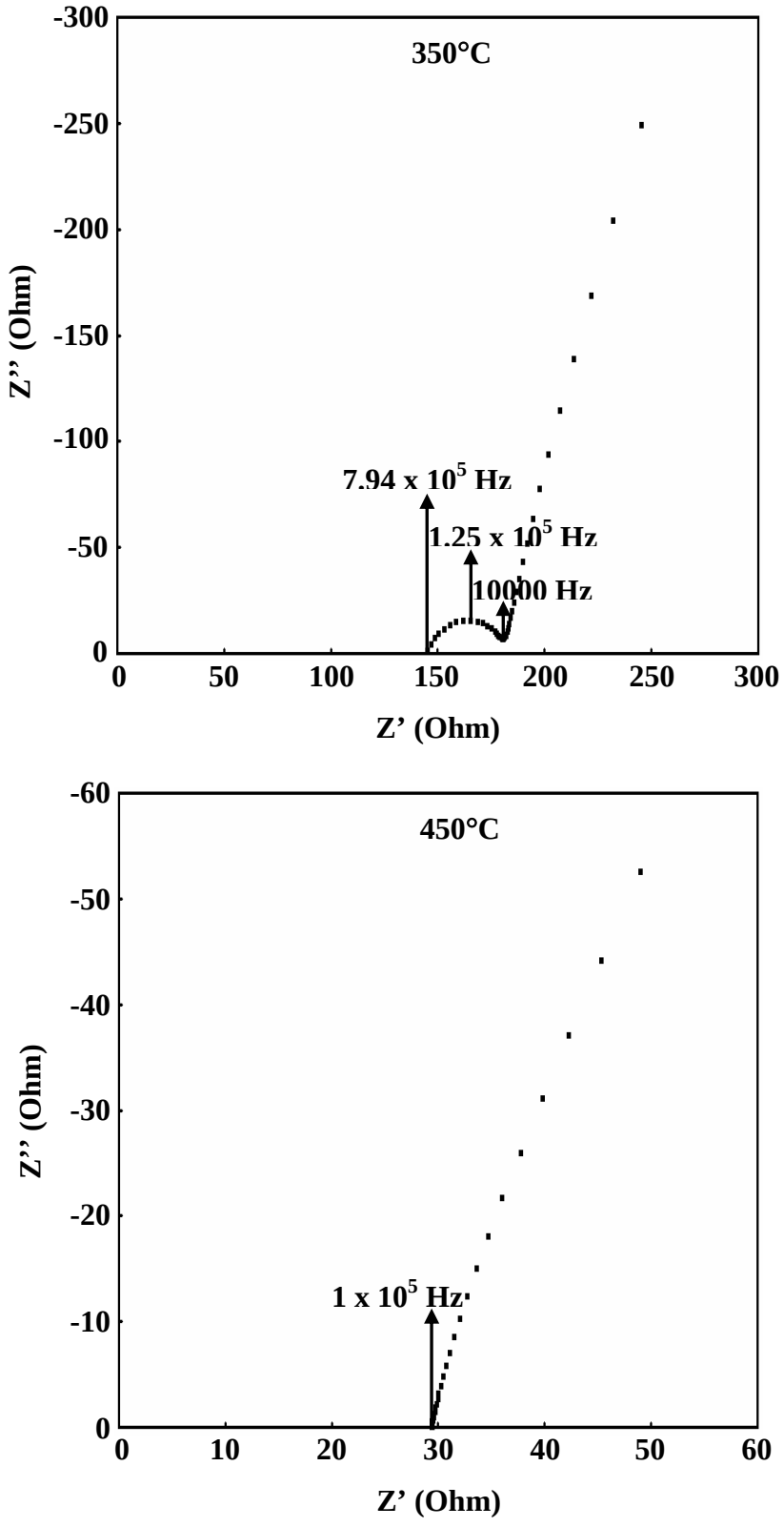

Figure 26 (Continued)

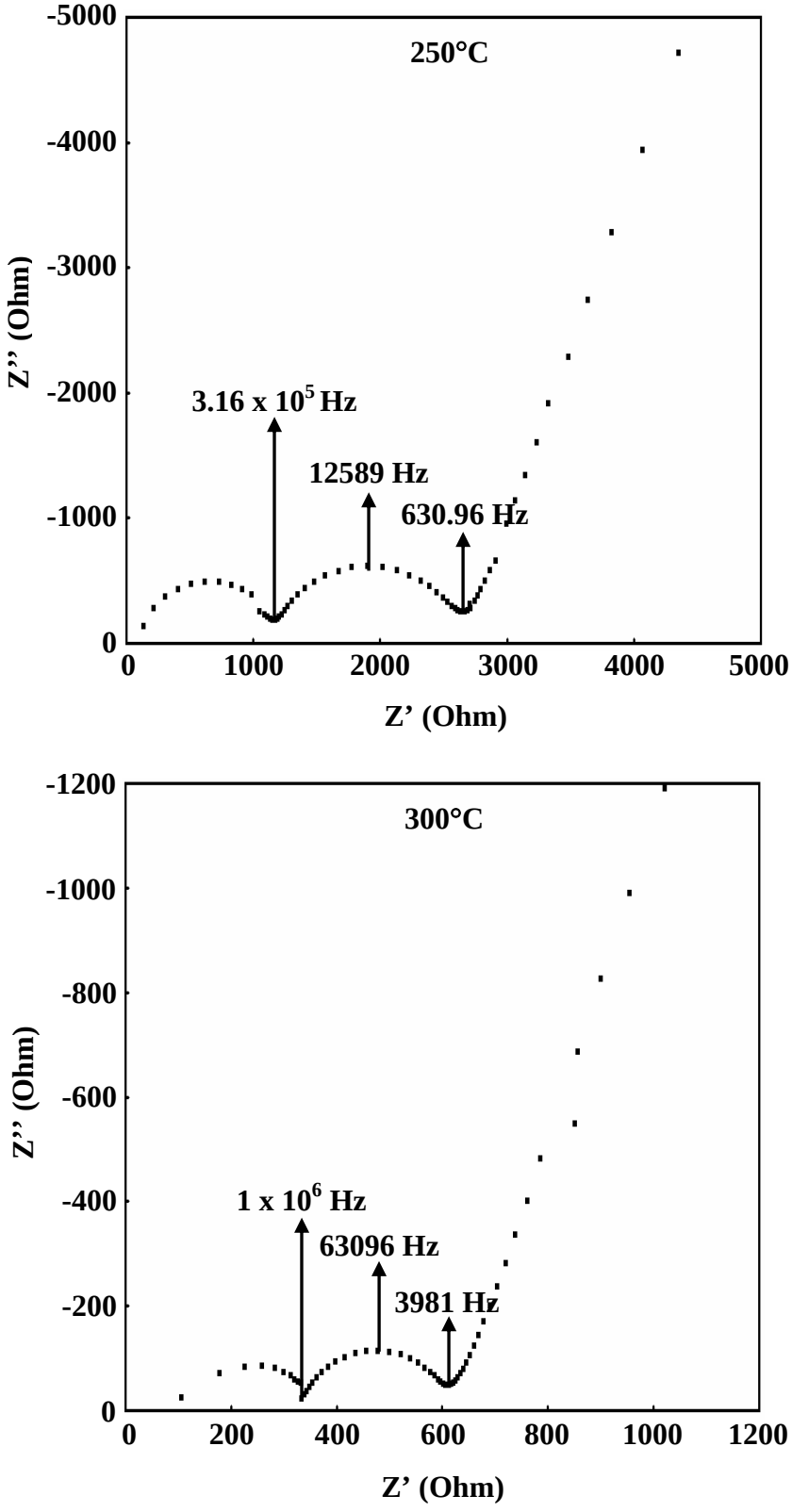

Figure 27 Impedance spectra of $Ce_{0.90}Sm_{0.10}O_{2-\delta}$ pellet which calcined at 600°C for 2 h in air and sintered at 1500°C for 5 h in air

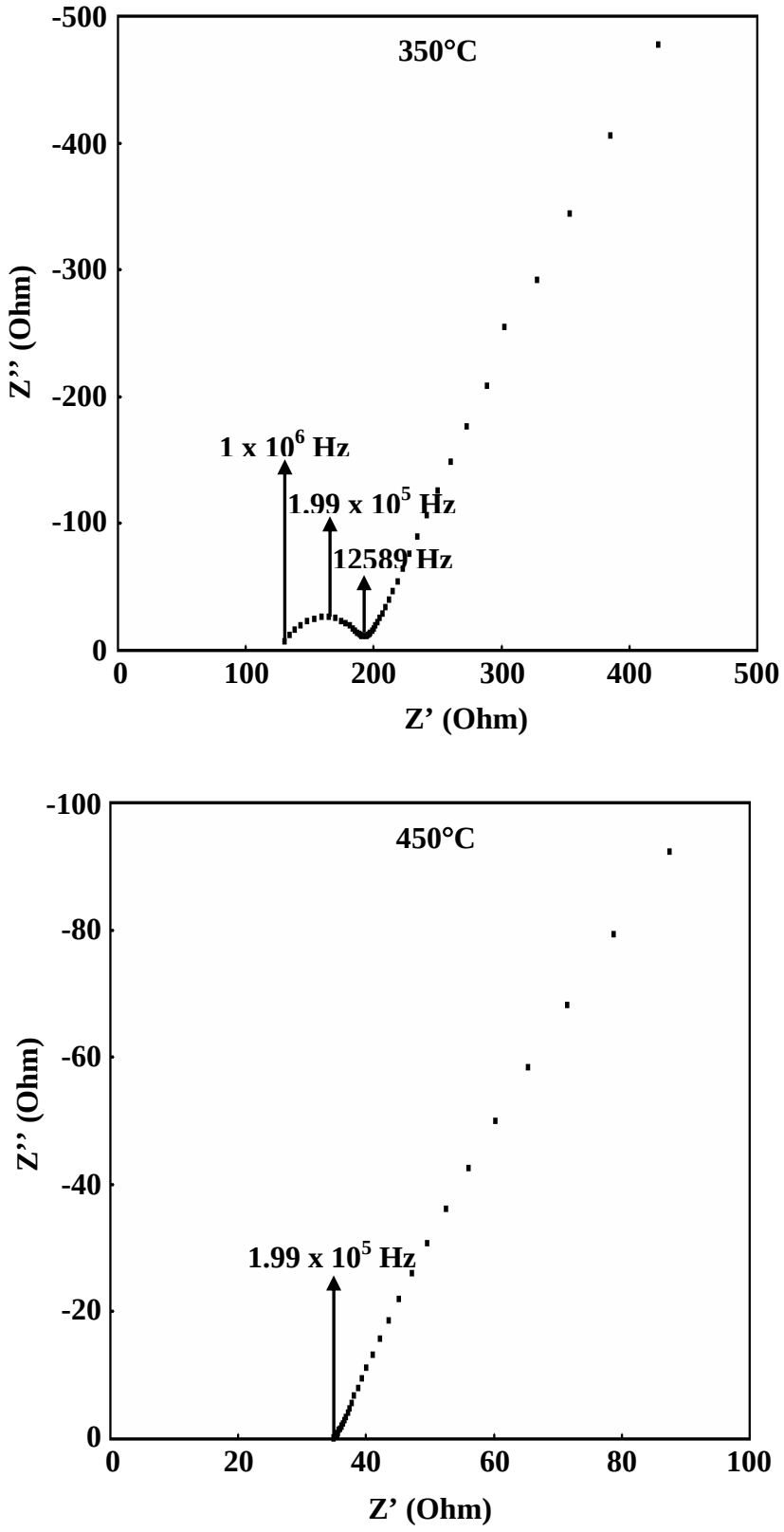

Figure 27 (Continued)

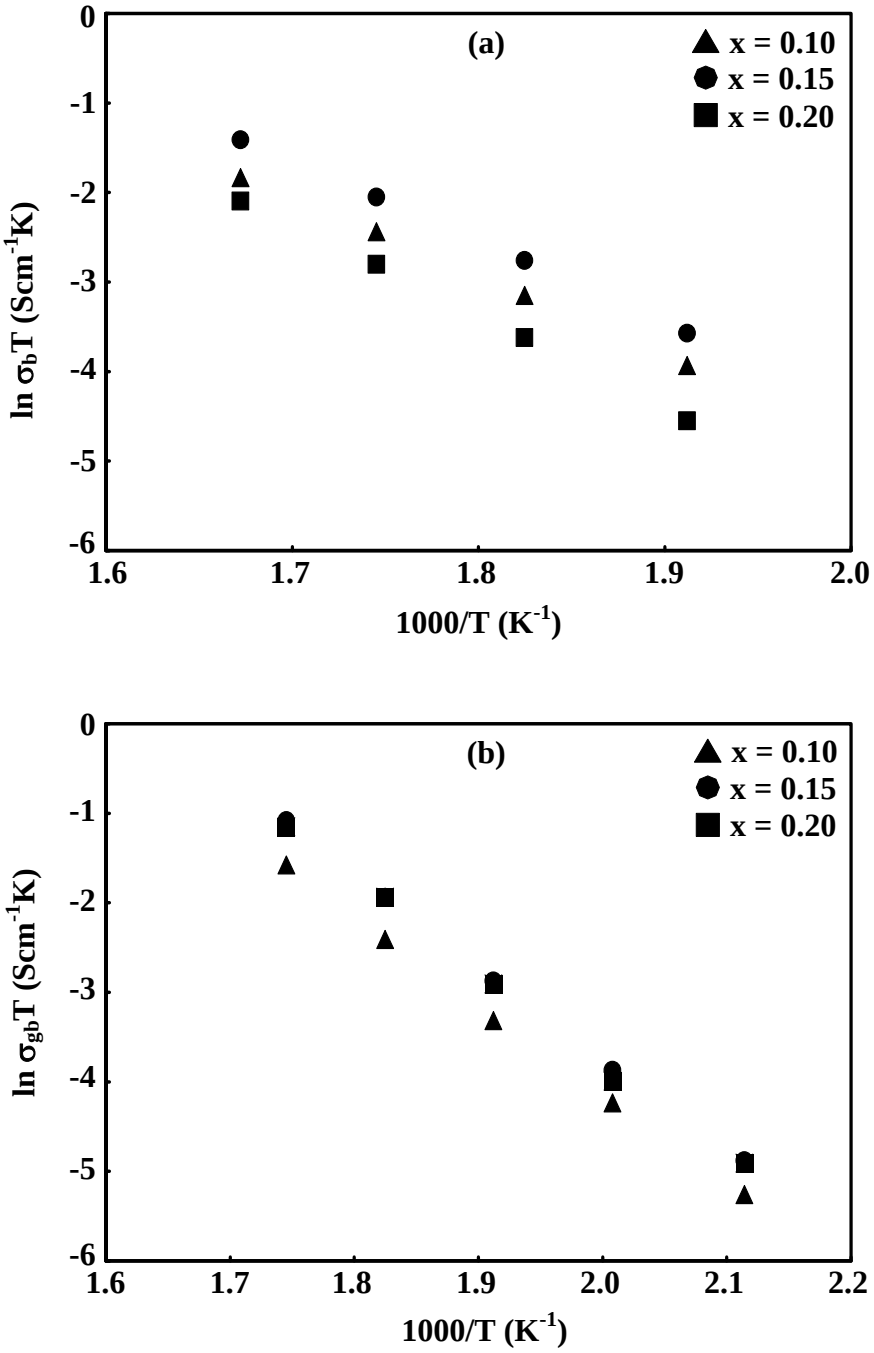

Figure 28 Arrhenius plot of (a) bulk and (b) grain boundary conductivities of $Ce_{1-x}Gd_xO_{2-\delta}$ pellets which calcined at 600°C for 2 h in air and sintered at 1500°C for 5 h in air

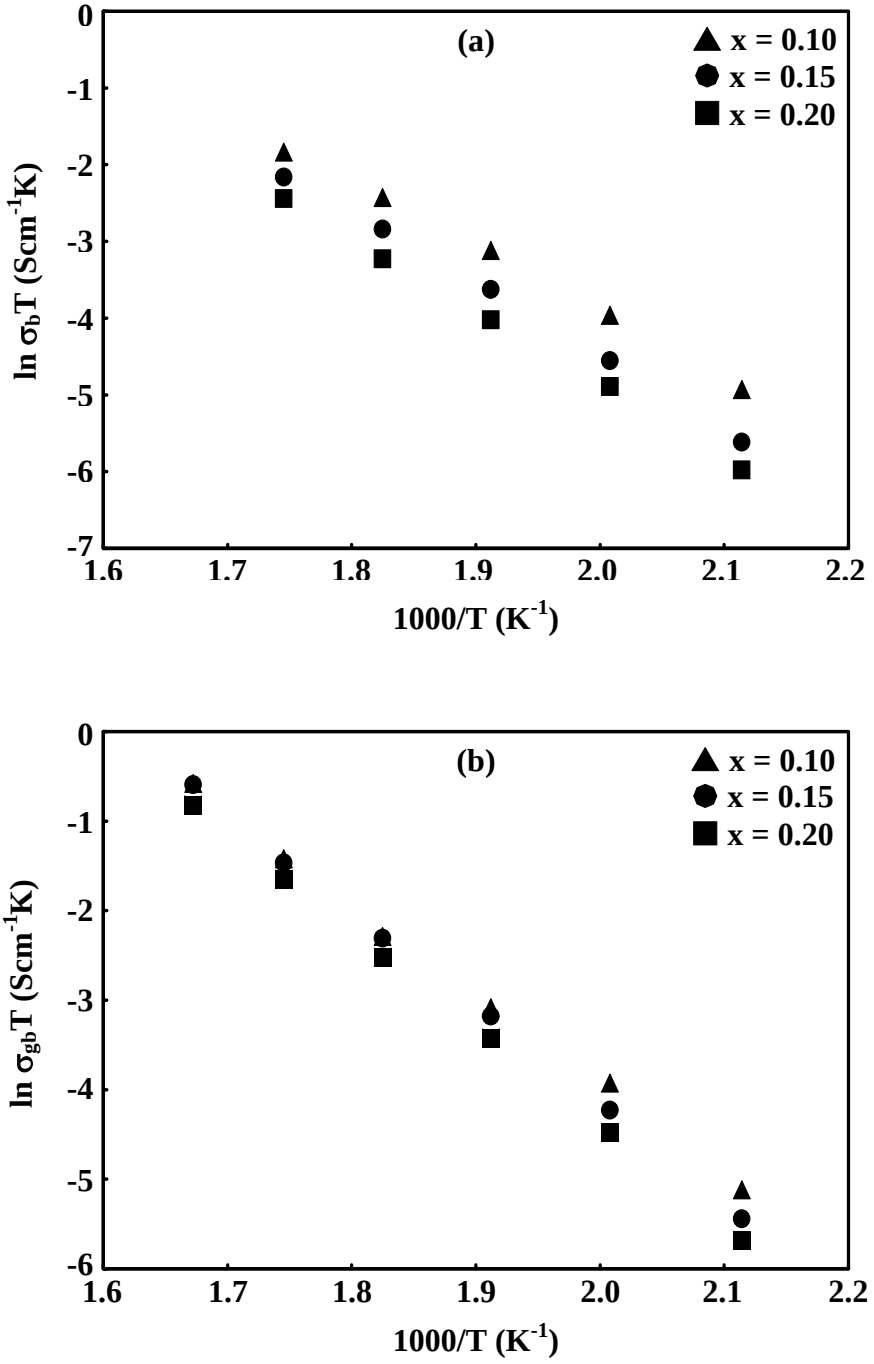

Figure 29 Arrhenius plot of (a) bulk and (b) grain boundary conductivities of $Ce_{1-x}Sm_xO_{2-\delta}$ pellets which calcined at 600°C for 2 h in air and sintered at 1500°C for 5 h in air

Figures 28 and 29 show the bulk and grain boundary conductivities Arrhenius plots of $Ce_{1-x}Gd_xO_{2-\delta}$ and $Ce_{1-x}Sm_xO_{2-\delta}$ pellets, respectively. The conductivities and activation energies were calculated based on the Arrhenius equation as shown below;

$$\sigma T = A\exp(-E_a/kT)$$

It was found that the bulk conductivity (σ_b) of the $Ce_{1-x}Gd_xO_{2-\delta}$ pellet was followed in the order of x; 0.15 > 0.10 > 0.20. This is expected because the increase amount of Gd more than 0.15 results in defect association and the amount of Gd at 0.10 is too small concentration to produce oxygen ion vacancies, resulting in the decrease of ionic conductivity. The grain boundary conductivity (σ_{gb}) of the $Ce_{1-x}Gd_xO_{2-\delta}$ pellet was followed in the order of x; 0.15 = 0.20 > 0.10. In the $Ce_{1-x}Sm_xO_{2-\delta}$ pellets, the bulk conductivity (σ_b) and the grain boundary (σ_{gb}) was followed in the same order of x; 0.10 > 0.15 > 0.20, especially at higher temperature.

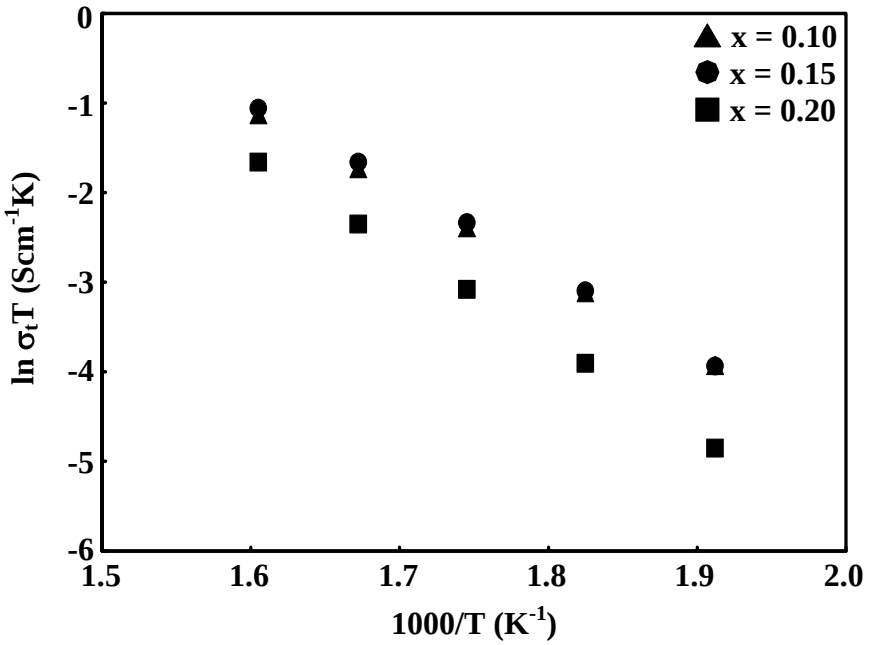

Figure 30 Arrhenius plot of total conductivity of $Ce_{1-x}Gd_xO_{2-\delta}$ pellets which calcined at 600°C for 2 h in air and sintered at 1500°C for 5 h in air

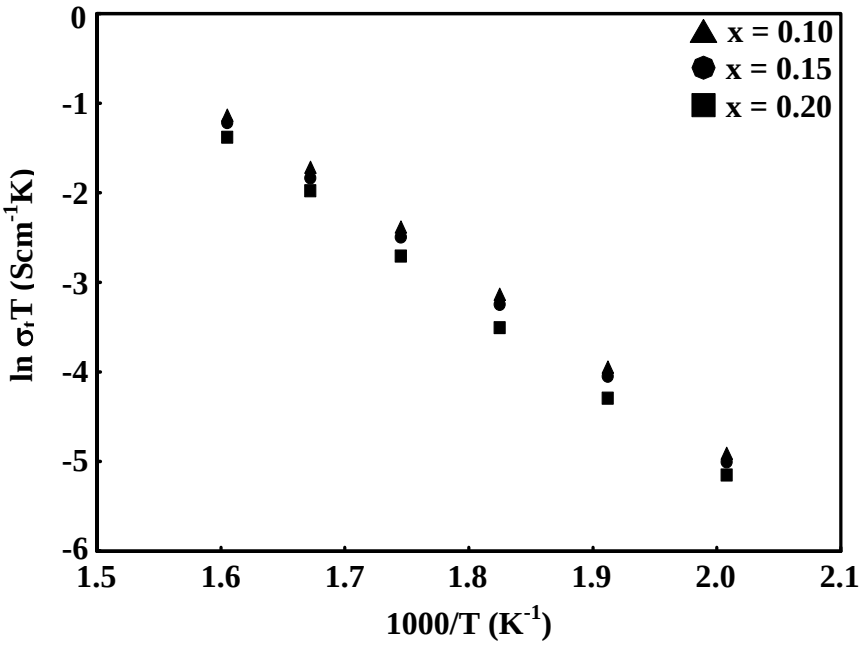

Figure 31 Arrhenius plot of total conductivities of $Ce_{1-x}Sm_xO_{2-\delta}$ pellets which calcined at 600°C for 2 h in air and sintered at 1500°C for 5 h in air

Figures 30 and 31 illustrate the temperature dependence of the total conductivities of $Ce_{1-x}Gd_xO_{2-\delta}$ and $Ce_{1-x}Sm_xO_{2-\delta}$ pellets, respectively. The results show that the $Ce_{0.85}Gd_{0.15}O_{2-\delta}$ and $Ce_{0.90}Sm_{0.10}O_{2-\delta}$ pellets give the largest ionic conductivity. The bulk, grain boundary and total conductivities at 600°C of $Ce_{1-x}Gd_xO_{2-\delta}$ and $Ce_{1-x}Sm_xO_{2-\delta}$ pellets are shown in Tables 6 and 7.

Table 6 The bulk, grain boundary, and total conductivities at 600°C of $Ce_{1-x}Gd_xO_{2-\delta}$ pellets

x	Conductivity (S/cm)		
	Bulk	Grain boundary	Total
0.10	0.0201	0.0902	0.0246
0.15	0.0348	0.1847	0.0302
0.20	0.0334	0.1814	0.0011

Table 7 The bulk, grain boundary, and total conductivities at 600°C of $Ce_{1-x}Sm_xO_{2-\delta}$ pellets

x	Conductivity (S/cm)		
	Bulk	Grain boundary	Total
0.10	0.0298	0.1179	0.0284
0.15	0.0383	0.1843	0.0255
0.20	0.0295	0.1587	0.0222

The activation energies of $Ce_{1-x}Gd_xO_{2-\delta}$ and $Ce_{1-x}Sm_xO_{2-\delta}$ pellet samples were shown in Tables 8 and 9, respectively.

Table 8 Activation energies of $Ce_{1-x}Gd_xO_{2-\delta}$ pellets

x	Activation energy (eV)		
	Bulk	Grain boundary	Total
0.10	0.7659	0.8601	0.7868
0.15	0.7847	0.8919	0.8101
0.20	0.8918	0.8953	0.8947

Table 9 Activation energies of $Ce_{1-x}Sm_xO_{2-\delta}$ pellets

x	Activation energy (eV)		
	Bulk	Grain boundary	Total
0.10	0.7251	0.8669	0.8155
0.15	0.8092	0.9351	0.7652
0.20	0.8197	0.9439	0.7653

CONCLUSION

An easy, inexpensive and straightforward of metal complex method can be carried out to prepare CeO_2 and $Ce_{1-x}Gd_xO_{2-\delta}$ and $Ce_{1-x}Sm_xO_{2-\delta}$ powders. The structures of pure cerium complex can be proposed as four coordinated cerium ion binding to TEA molecule [Ce(TEA)] and five coordinated cerium ion with TEA and Cl^- ligands [Ce(TEA)Cl]. The obtained ceramic powders are pure, homogeneous, and nanosize. The appropriate temperature for calcining metal complex into ceramic powders is started at 600°C. The effects of calcination temperatures observed clarity match to the theories that the agglomeration and densification are increased with increasing the calcination temperature. From the impedance spectroscopy, the largest conductivity of $Ce_{1-x}Gd_xO_{2-\delta}$ and $Ce_{1-x}Sm_xO_{2-\delta}$ is found for the 0.15 mol% Gd substitution ($\sigma_{600°C}$ = 0.0302 S/cm) and 0.10 mol% Sm substitution ($\sigma_{600°C}$ = 0.0284 S/cm), respectively.

LITERATURE CITED

Badwal, S.P.S. and K. Foger. 1996. Solid Oxide Electrolyte Fuel Cell Review. **Ceram. Int.**, 257-265.

Balazs, G.B. and R.S. Glass. 1995. Ac impedance studies of rare earth oxide doped ceria. **Solid state ionics**. 76: 155-162.

Boudghene S.A. and E. Traversa. 2002. Solid oxide fuel cells (SOFCs): a review of an environmentally clean and efficient source of energy. **Renewable Sustainable Energy Rev.**, 6: 433-455.

Chen, M., B.H. Kim, Q. Xu, B.K. Ahn, W.J Kang and D.P. Huang. 2008. Synthesis and electrolytes by urea-combustion technique. **Ceram. Int**., *In press*.

Chinarro, E., J.R. Jurado, and M.T. Colomer. 2007. Synthesis of ceria-based electrolyte nanometric powders by urea-combustion technique. **J. Eur. Ceram. Soc**., 27: 3619-3623.

Daniela, T., T. Alessandro, L. Jordi, L. Carla and D. Giuliano. 1998. The Synthesis and Characterization of Mesoporous High-Surface Area Ceria Prepared Using a Hybrid Organi/Inorganic Route. **J. Catal.**, 178: 299-308.

Dikmen, S., P. Shuk, M. Greenblatt and H. Goomez. 2002. Hydrothermal synthesis and properties of $Ce_{1-x}Gd_xO_{2-\delta}$ solid solutions. **Solid State Science.**, 4: 585-590.

Dong, Y.C. and H.L. Eil. 2004. Microwave-induced combustion synthesis of $Ce_{1-x}Sm_xO_{2-x/2}$ powder and its characterization. **J. Alloys Compd.**, 374: 69-73.

Dos Santos, M.I., R.C. Lima, C.S. Riccardi, R.L. Tranquilin, P.R. Bueno, J.A. Varela and E. Longo. 2008. Preparation and characterization of ceria nanospheres by microwave-hydrothermal method. **Mater. Lett.**, 62: 4509-4511.

Dudek, M. 2007. Ceramic oxide electrolytes based on CeO_2-Preparation, properties and possibility of application to electrochemical devices**. J. Eur. Ceram. Soc.**, In press.

Esposito, V. and E. Traversa. 2008. Design of electroceramics for solid oxides fuel cell applications: playing with ceria. **J. Am. Ceram. Soc.**, 91(4) 1037-1051.

Esposito, V., F.C. Fonseca, D.Z. Florio, M. Zunic, R. Muccillo and E. Traversa. 2000. Fabrication of $Ce_{1-x}Gd_xO_{2-0.5x}$ Electrolyte with Tunable Dense Microstructures for IT-SOFC Applications. **ECS Trans.**, 7 (1): 2093-2101.

Feng-Wang, W., C. Songying, C. Soofin. 2004. Gd^{3+} and Sm^{3+} co-doped ceria based electrolytes for intermediate temperature solid oxide fuel cells. **Electrochem. Commun.**, 6: 743-746.

Fu, Y.P. 2007. Preparation and Characterization of Samaria-Doped Ceria Electrolyte Materials for Solid Oxide Fuel cells. **J. Am. Ceram. Soc.**, 00 [0]: 1-5.

Fu, Y.P. 2008. Microwave-induced combustion synthesis and ionic conductivity of $Ce_{0.8}(Gd_{0.2-x}Sm_x)O_{1.90}$ ceramics. **Ceram. Int.**, 34: 2051-2057.

Fuentes, R.O. and R.T. Baker. 2008. Synthesis and properties of Gadolinium-doped ceria solid solutions for IT-SOFC electrolytes. **Int. J. Hydrogen Energy**, 33: 3480-3483.

Fuentes, R.O. and R.T. Baker. 2009. Structural, morphological and electrical properties of $Gd_{0.1}Ce_{0.9}O_{1.95}$ prepared by a citrate complexation method. **J. Power Sources**, 186: 268-277.

Gao, R. and Z. Mao. 2007. Sintering of $Ce_{0.8}Sm_{0.2}O_{1.9}$. **J. Rare Earths**, 25: 364-367.

Grover, V. and A.K. Tyagi. 2004. Phase relations, lattice thermal expansion in CeO_2-Gd_2O_3 system, and stabilization of cubic gadolinia. **Mater. Res. Bull.**, 39: 859-866.

Guan, X., Z. Heping, L. Zhihui, W. Yanan and Z. Jun. 2008. Preparation of Gd^{3+} and Y^{3+} co-doped ceria-based electrolytes for intermediate temperature solid oxide fuel cells. **Mater. Res. Bull.**, 43: 1046-1054.

Haile, S.M. 2003. Fuel Cell materials and components. **Acta Matter.**, 51: 5981-6000.

Hari Prasad, D., J.W. Son, B.K. Kim, H.W. Lee and J.H. Lee. 2008. Synthesis of nano-crystalline $Ce_{0.9}Gd_{0.1}O_{1.95}$ electrolyte by novel sol-gel thermolysis process for IT-SOFCs. **J. Eur. Ceram. Soc.**, 28: 3107-3112.

Hideaki, I., N. Toshifumi and T. Hiroaki. 1998. Sintering behaviors of ceria and gadolinia-doped ceria. **Solid State Ionics.**, 106: 263-268.

Hu, J.D., Y.X. Li, X.Z. Zhou and M.X. Cai. 2007. Preparation and characterization of ceria nanoparticles using crystalline hydrate cerium propionate as precursor. **Mater. Lett.**, 61: 4989-4992.

Hui, S., J. Roller, S. Yick, X. Zhang, C.D. Petit, Y. Xie, R. Maric and D. Ghosh. 2007. A brief review of the ionic conductivity enhancement foe selected oxide electrolytes. **J. Power Sources**, 172: 493-502.

Ifan, E.L. and A.K. John. 2006. Ionic conductivity of $Ce_{1-x}Nd_xO_{2-x/2}$. **Solid State Ionics**, 177: 669-676.

Im, J.M., H.J. You, Y.S. Yoon and D.W. Shin. 2007. Synthesis of nano-sized gadolinia doped ceria powder by aerosol flame deposition. **J. Eur. Ceram. Soc.**, 27: 3671-3675.

Jadhav, L.D., M.G. Chourashiya, K.M. Subhedar, A.K. Tyagi and J.Y. Patil. 2008. Synthesis of nanocrystalline Gd doped ceria by combustion technique. **J. Alloys Compd.**, *In press*.

Jasper, A., J.A. Kilner and D.W. McComb. 2008. TEM and impedance spectroscopy of doped ceria electrolytes. **Solid State Ionics**, *In press*.

Ji, Y., J. Liu, T. He, L. Cong, J. Wang and W. Su. 2003. Single intermedium-temperature SOFC prepared by glycine-nitrate process. **J. Alloys Compd.**, 353: 257-262.

Ji, Y., J. Liu, T. He, J. Wang and W. Su. 2005. The effect of Pr co-dopant on the performance of solid oxide fuel cells with Sm-doped ceria electrolyte. **J. Alloys Compd.**, 389: 317-322.

Ji-Guang, L., I. Takayasu and M. Toshiyuki. 2004. Low temperature processing of dense samarium-doped CeO_2 ceramic: sintering and growth behaviors. **Acta Mater.**, 52: 2221-2228.

Jigui, C., Z. Shaowu and F. Xiaohong. 2002. On the green density, sintering behavior and electrical property of tape cast $Ce_{0.9}Gd_{0.1}O_{1.95}$ electrolyte films. **Mater. Res. Bull.**, 37: 2437-2446.

Jong, M.I., J.Y. Hyun, S.Y. Yong and W.S. Dong. 2008. Synthesis of nano-crystalline $Gd_{0.1}Ce_{0.9}O_{2-x}$ for IT-SOFC by aerosol flame deposition. **Ceram. Int.**, 34: 877-88.

Kim, N., B.H. Kim and D. Lee. 2000. Effect of co-dopant addition on properties of gadolinia-doped ceria electrolyte. **J. Power Sources**, 90: 139-143.

Kim, S. and J. Maier. 2002. On the conductivity mechanism of nanocrystalline ceria. **J. Electrochem. Soc.**, 149 (10) J73-J83.

Kuharuangrong, S. 2007. Ionic conductivity of Sm, Gd, Dy and Er-doped ceria. **J. Power Sources**, 171: 506-510.

Laobuthee, A., S. Wongkasemjit, E. Traversa and R.M. Laine. 2000. $MgAl_2O_4$ spinel powders from oxide one pot synthesis (OOPS) process for ceramic humidity sensors. **J. Eur. Ceram. Soc.**, 20: 91-97.

Lee, J.S., K.H. Choi, B.K. Ryu, B.C. Shin and I.S. Kim. 2004. Effects of alumina additions on sintering behavior of gadolinia-doped ceria. **Ceram. Int.**, 30: 807-812.

Lenka, R.K., T. Mahata, P.K. Sinha and B.P. Sharma. 2006. Combustion synthesis, powder characteristics, and shrinkage behavior of a gadolinia-ceria system. **J. Am. Ceram. Soc.**, 89: 3871-3873.

Leoni, M., R.S. Maggio, S. Polizzi and P. Scardi. 2004. X-ray diffraction methodology for the microstructural analysis of nanocrystalline powders: application to cerium oxide. **J. Am. Ceram. Soc.**, 87(6): 1133-1140.

Li, J.G., T. Ikegami and T. Mori. 2004. Low temperature processing of dense samarium-doped CeO_2 ceramics: sintering and grain growth behaviors. **Acta Mater.**, 52: 2221-2228.

Liu, G.C., L.M. Chen, X.C. Duan and D.W. Liang. 2008. Synthesis and characterization of Sm^{3+}-doped CeO_2 powders. **Trans. Nonferrous Met. Soc. Chaina**, 18: 897-903.

Ma, J., T.S. Zhang, L.B. Kong, P. Hing and S.H. Chan. 2004. $Ce_{0.8}Gd_{0.2}O_{2-\delta}$ ceramics derived from commercial submicron-sized CeO_2 and G_2O_3 powders for use as electrolytes in solid oxide fuel cells. **J. Power Sources**, 132: 71-76.

Maffei, N. and A.K. Kuriakose. 1998. Solid oxide fuel cells of ceria doped zith gadolinium and praseodymium. **Solid State Ionics.**, 107: 67-71.

Mahata, T., G. Das, R.K. Mishra and B.P. Sharma. 2005. Combustion synthesis of gadolinia-doped ceria powder. **J. Alloys Compd.**, 391: 129-135.

Matteo, L., D.M. Rosa, P. Stefano and S. Paolo. 2004. X-ray diffraction Methodology for the Microstructural Analysis of Nanocrystalline Powders: Application to Cerium Oxide. **J. Am. Ceram. Soc.**, 87(6): 1113-1140.

Minh, N.Q. 1993. Ceramic Fuel Cells**. J. Am. Ceram. Soc.**, 76 [3]: 563-588.

Omar, S., E.D. Wachsman and J.C. Nino. 2008. Higher conductivity Sm^{3+} and Nd^{3+} co-doped ceria-based electrolyte materials. **Solid state ionics.**, 178: 1890-1897.

Peng, C. and Z. Zhen, Nitrate-citrate combustion synthesis of $Ce_{1-x}Gd_xO_{2-x/2}$ powder and its characterization. **Ceram. Int.**, *In press*.

Perez-Coll, D., D. Marrero-Lopez, P. Nunez, S. Pinol and J.R. Frade. 2006. Grain boundary conductivity of $Ce_{0.8}Ln_{0.2}O_{2-\delta}$ ceramics (Ln = Y, La, Gd, Sm) with and without Co-doping. **Electrochim. Acta**, 51: 6463-6469.

Perez-Coll, D., P. Nunez, J.R. Frade and J.C.C. Abrantes. 2003. Conductivity of CGO and CSO ceramics obtained from freeze-dried precursors. **Electrochim. Acta**, 48: 1551-1557.

Purohit, R.D., B.P. Sharma, K.T. Pillai and A.K. Tyagi. 2001. Ultrafine ceria poders via glycine-nitrate combustion. **Mater. Res. Bull.**, 36: 2711-2721.

Rangsapram, S. 2001. **Characteristic of Lanthanum Aluminate as as Electrolyte in Solid Oxide Fuel Cell**. M.S. Thesis, Chulalongkorn University.

Raja, K.L., M. Tarasankar, K. S. Pankaj and P.S. Beant. 2006. Combustion Synthesis, powder Characteristics, and Shrinkage Behavior of a Gadolinia-Ceria System. **J. Am. Ceram. Soc.**, 89: 3871-3873.

Rey, J.F.Q. and E.N.S. Muccillo. 2004. Lattice parameters of yttria-doped ceria solid electrolytes. **J. Eur. Ceram. Soc.**, 24: 1287-1290.

Sakai, N., Y.P. Xiong, K. Yamaji, H. Yokokaea, Y. Terashi and H. Seno. 2006. Anomalous conductivity and microstructure in gadolinium doped ceria prepared from nano-sized powder. **Solid State Ionics**, 177: 2503-2507.

Sangtae, K. and M. Joachim. 2002. On the Conductivity Mechanism of Nanocrystalline Ceria. **Electrochem. Soc. Interface**, 149 (10): J73-J83.

Seung, H.J., P. Muralidharan, D.K. Kim. 2008. Electrical characterization of dense and porous nanocrystalline Gd-doped ceria electrolytes. **Solid State Ionics**, 178: 1990-1997.

Shaowu, Z., X. Changrong and M. Guangyao. 2003. Effect of Gd (Sm) doping on properties of ceria electrolyte for solid oxide fuel cells. **J. Power Sources**, 115: 44-48.

Sha, X., Z. Lu, X. Huang, J. Miao, Z. Liu, X. Xin, Y. Zhang and W. Su. 2007. Influence of the sintering temperature on electrical property of the $Ce_{0.8}Sm_{0.1}Y_{0.1}O_{0.19}$ electrolyte. **J. Alloys Compd.**, 433: 274-278.

Snezana, B.B., R.D. Dejan, P.Z. Slavica, Z.M. Branko, Z. Matvei and A. Fritz. 2007. Doped and co-doped CeO_2: Preparation and properties. **Ceram. Int.**, *In press.*

Souza, E.C.C. and E.N.S. Muccillo. 2008. Effect of solvent on physical properties of samaria-doped ceria prepared by homogeneous precipitation. **J. Alloys Compd.**, *In press*.

Thangadurai, V. and P. Kopp. 2007. Chemical synthesis of Ca-doped CeO_2 – Intermediate temperature oxide ion electrolytes. **J. Power Sources**, 168: 178-183.

Tok, A.I.Y., L.H. Luo and F.Y.C. Boey. 2004. Carbonate Co-precipitation of Gd_2O_3-doped CeO_2 solid solution nano-particles. **Mater. Sci. Eng. A.**, 383: 229-234.

Torrens, R.S., N.M. Sammes and G.A. Tompsett. 1998. Characterisation of $(CeO_2)_{0.8}(GdO_{1.5})_{0.2}$ synthesised using various techniques. **Solid State Ionics**, 111: 9-15.

Trejo, E.R., J.S. Salazar, R.V. Morales, A.B. Rico, F.G. Garcia, C.F. Morales, J.C. Carvayar and G. Tavizon. 2007. Microstructure and electrical transport in nano-grain sized $Ce_{0.9}Gd_{0.1}O_{2-\delta}$ ceramics. **Solid State Chem.**, 180: 3093-3100.

Trovarelli, A. 2002. **Catalysis by Ceria and Related Materials**. Would Scientific Printers, Singapore.

Tsoga, A., A. Naoumidis, W. Jungen and D. Stover. 1999. Processing and Characterisation of Fine Crystalline ceria Gadolinia-Yttria Stabilized Zircona Powders. **J. Eur. Ceram. Soc.**, 19 (1999): 907-912.

Veranitisagul, C. 2008. **Preparation and Characterization of Ceria and Doped Ceria via Metal Organic Complex Method for Solid Oxide Fuel Cell Electrolyte Materials**. PhD. Thesis, University of Rome "Tor Vergata", Italy.

Wandekar, R.V., M. Ali, B.N. Wani and S.R. Bharadwaj. 2006. Physicochemical studies of NiO-GDC composites. **Mater. Chem. Phys.**, 99: 289-294.

Wang, S., J. Liu, J. Jia, C. Liao and C. Yan. 2008. Preparation of ceria with large particle size and high appearance density. **J. Rare Earths**, 26: 127-130.

Wang, S., T. Kobayashi, M. Dokiya and T. Hashimoto. 2000. Electrical and Ionic Conductivity of Gd-Doped Ceria. **J. Electro. Soc.**, 147 (10): 3606-3609.

Wang, Y., T. Mori, J.G. Li and T. Ikegami. 2002. Low-temperature synthesis of praseodymium-doped ceria nanopowders. **J. Am. Ceram. Soc.**, 85 (12) 3105-3107.

Yan, K., Q. Zhen and X. Song. 2007. Study on rare earth/alkaline earth oxide-doped CeO_2 solid electrolyte. **Rare Met.**, 26(4): 311.

Yuan, J., L. Jiang, H. Tianmin, W. Jinxia and S. Wenhui. 2005. The effect of Pr co-dopant on the performance of solid oxide fuel cells with Sm-doped ceria electrolyte. **J. Alloys Compd.**, 389: 317-322.

Yue, L. and X.M. Zhang. 2008. Structural characterization and photocatalytic behaviors of doped CeO_2 nanoparticles. **J. Alloys Compd.**, *In press*.

Zhan, Z., T.L. Wen, H. Tu and Z.Y. Lu. 2001. AC Impedance Investigation of Samarium-Doped Ceria**. J. Electrochem. Soc.**, 148 (5): A427-A432.

Zhang, T.S., J. Ma, L.B. Kong, P. Hing and J.A. Kilner. 2004. Preparation and mechanical properties of dense $Ce_{0.8}Gd_{0.2}O_{2-\delta}$ ceramics. **Solid State Ionics**, 167: 191-196.

APPENDIX

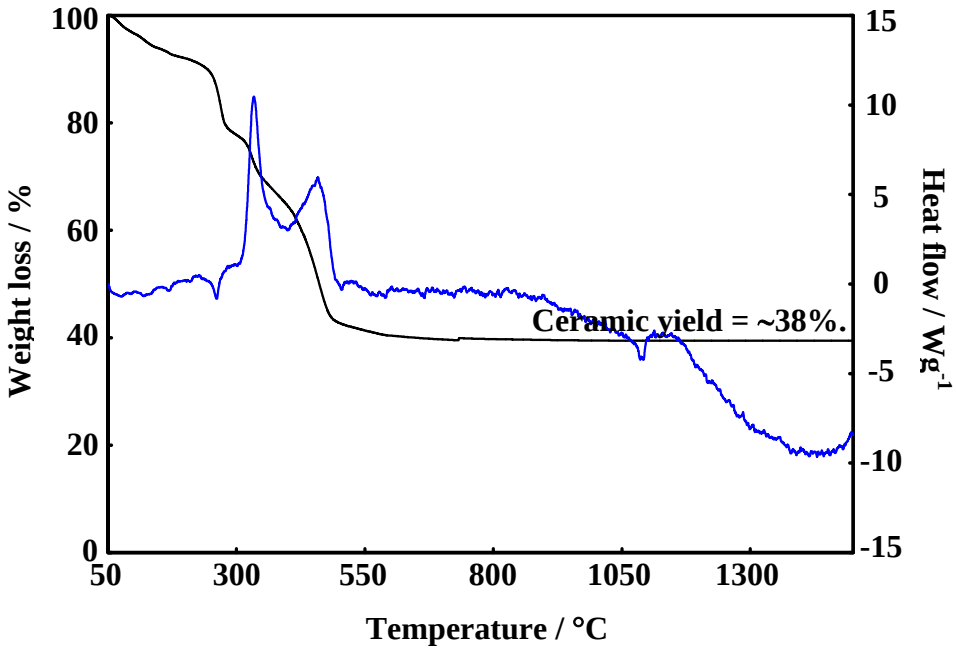

Appendix Figure 1 TGA/DSC thermogram of 15 mol% Gd-doped cerium complex

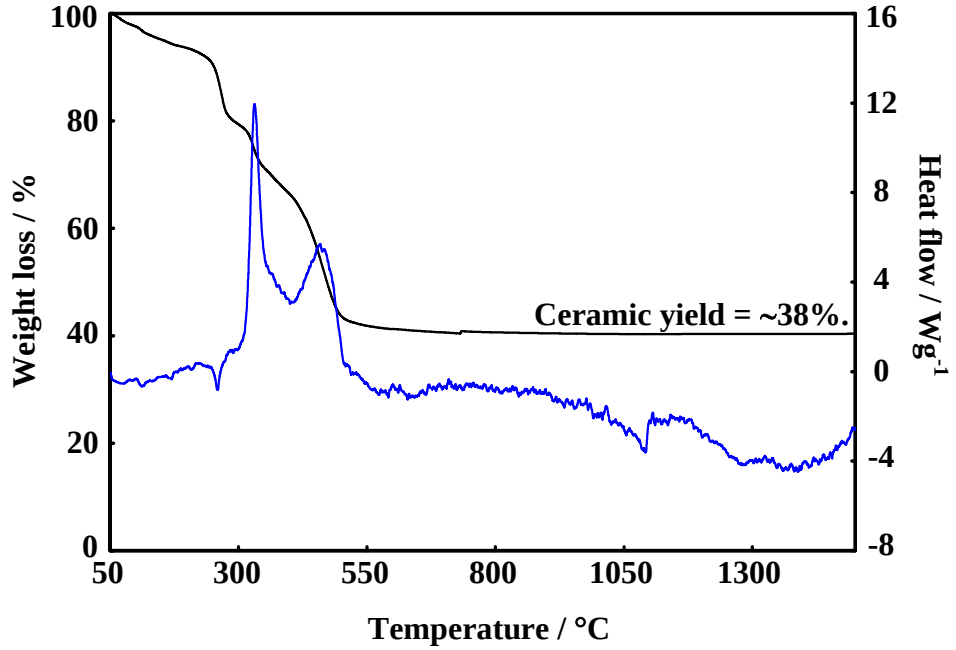

Appendix Figure 2 TGA/DSC thermogram of 20 mol% Gd-doped cerium complex

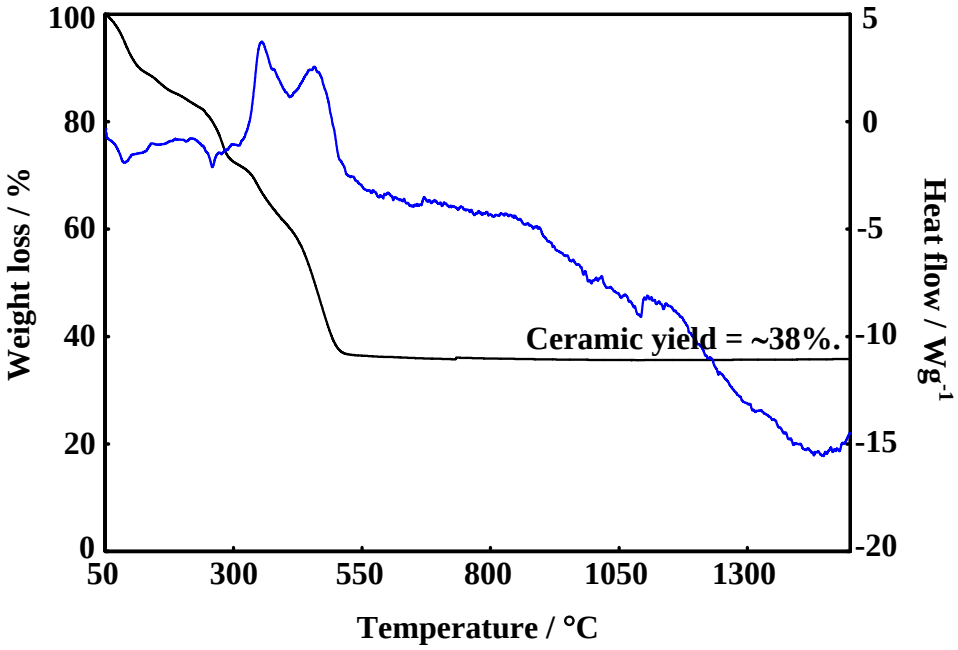

Appendix Figure 3 TGA/DSC thermogram of 15 mol% Sm-doped cerium complex

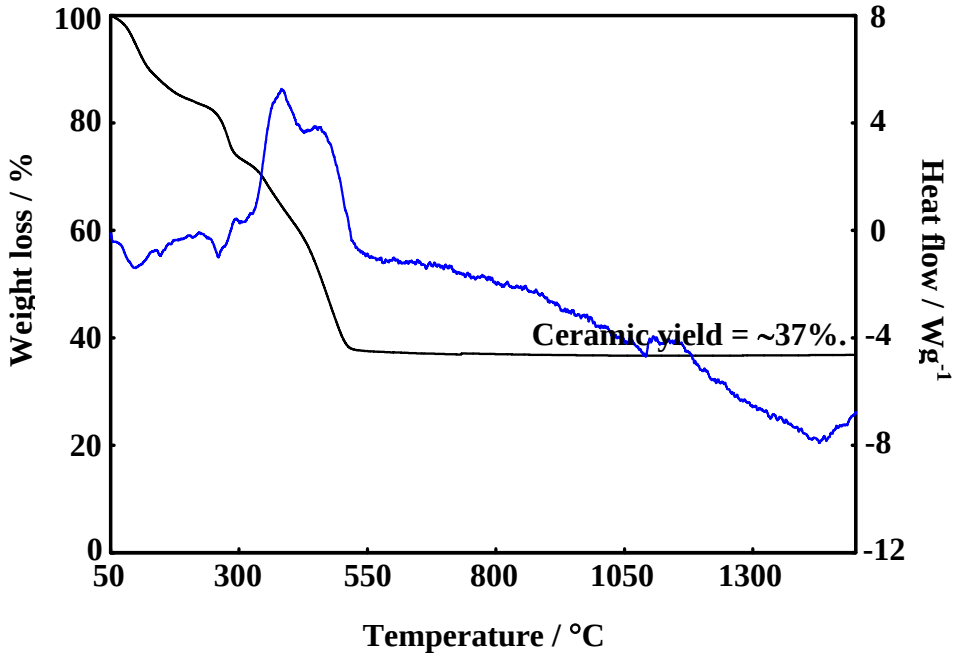

Appendix Figure 4 TGA/DSC thermogram of 20 mol% Sm-doped cerium complex

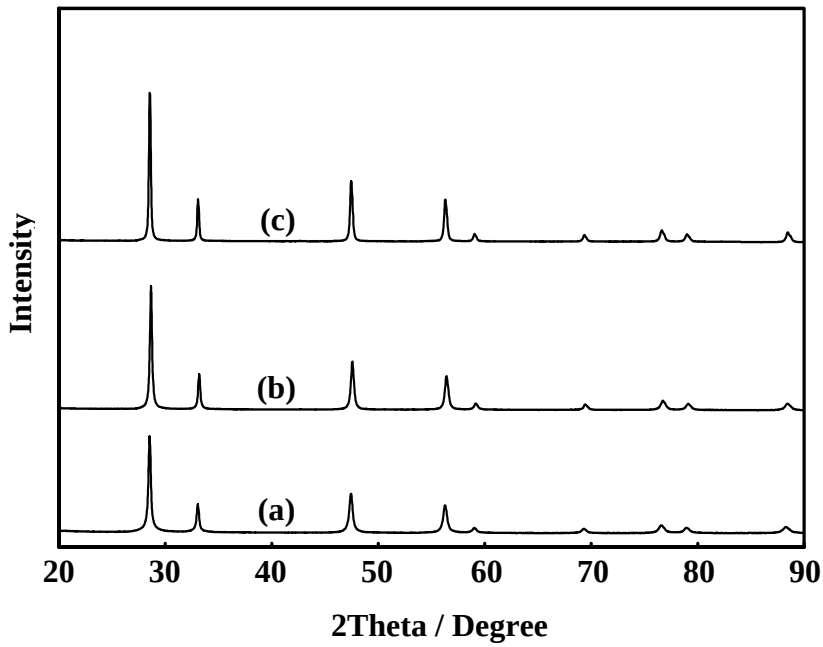

Appendix Figure 5 XRD patterns of $Ce_{0.85}Gd_{0.15}O_{2-\delta}$ powders calcined at (a) 600°C, (b) 800°C, and (c) 1000°C for 2 h in air

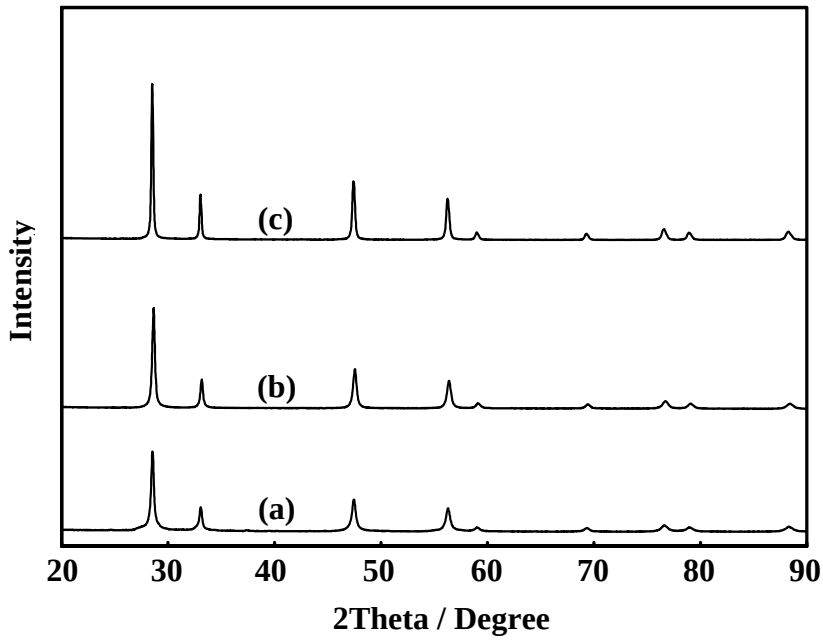

Appendix Figure 6 XRD patterns of $Ce_{0.80}Gd_{0.20}O_{2-\delta}$ powders calcined at (a) 600°C, (b) 800°C, and (c) 1000°C for 2 h in air

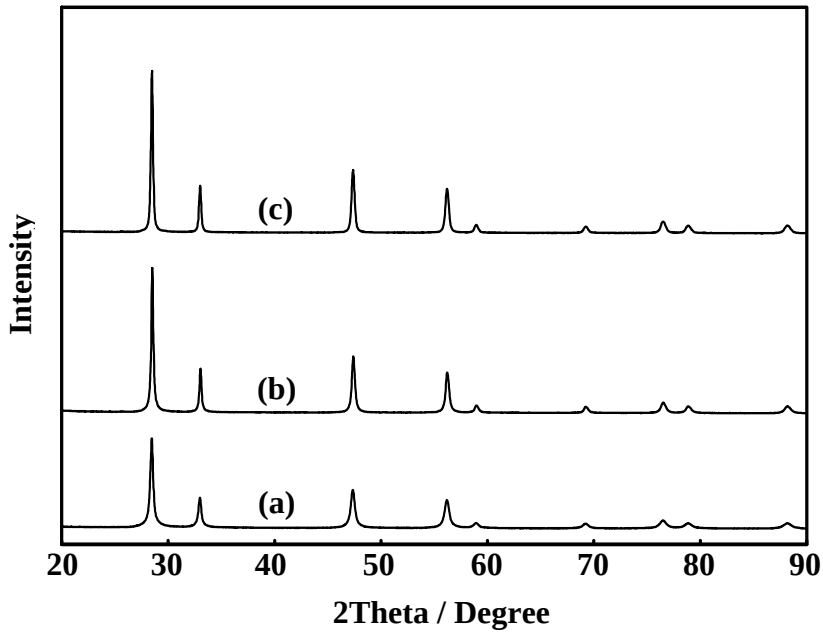

Appendix Figure 7 XRD patterns of $Ce_{0.85}Sm_{0.15}O_{2-\delta}$ powders calcined at (a) 600°C, (b) 800°C, and (d) 1000°C for 2 h in air

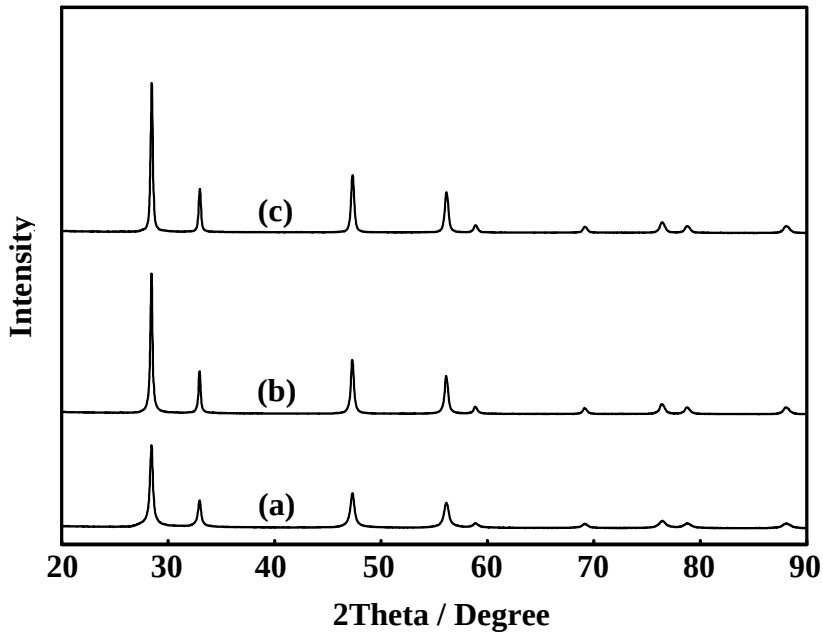

Appendix Figure 8 XRD patterns of $Ce_{0.80}Sm_{0.20}O_{2-\delta}$ powders calcined at (a) 600°C, (b) 800°C, and (c) 1000°C for 2 h in air

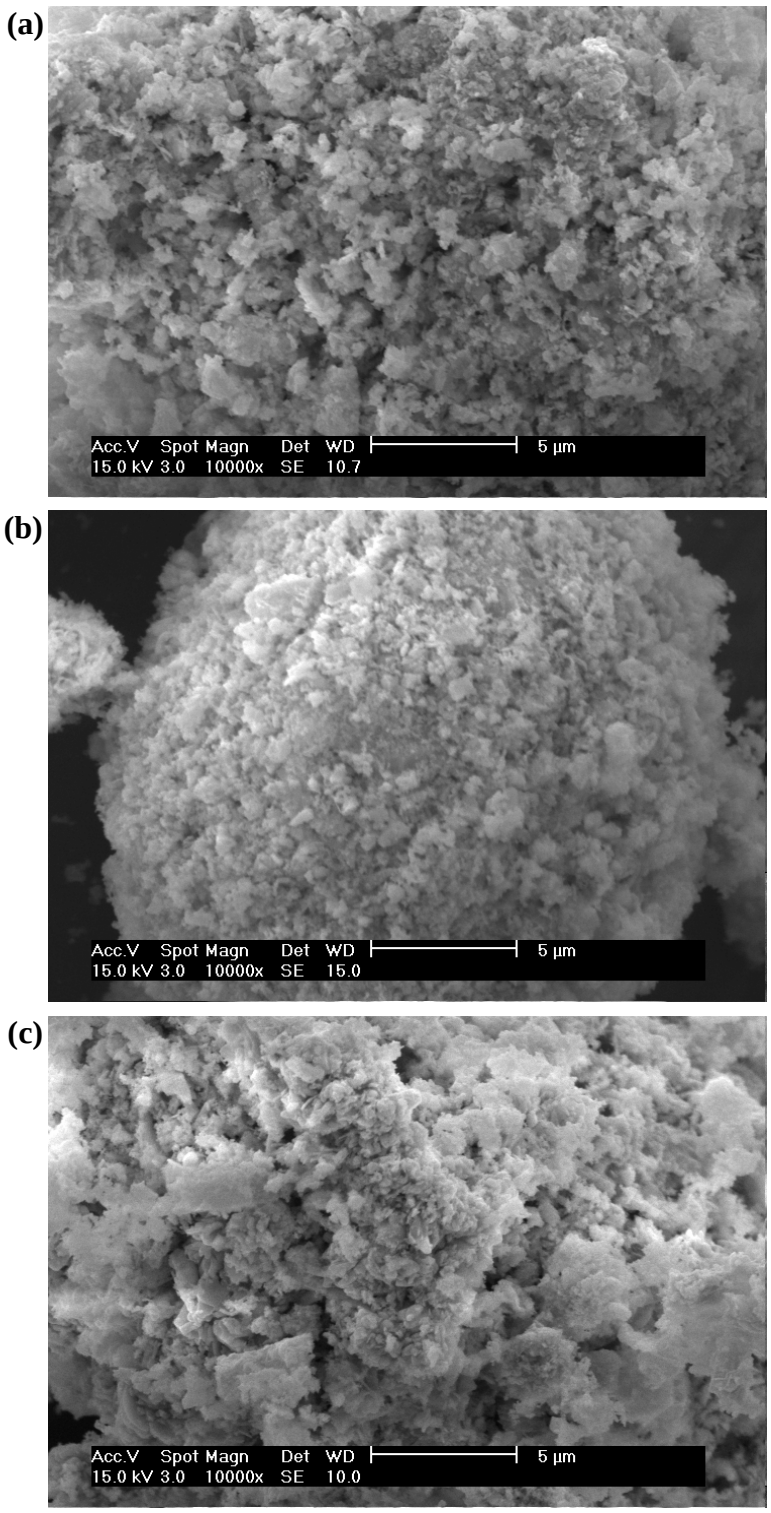

Appendix Figure 9 SEM micrographs of $Ce_{0.85}Gd_{0.15}O_{2-\delta}$ powders calcined for 2 h in air at (a) 600°C, (b) 800°C, and (c) 1000°C

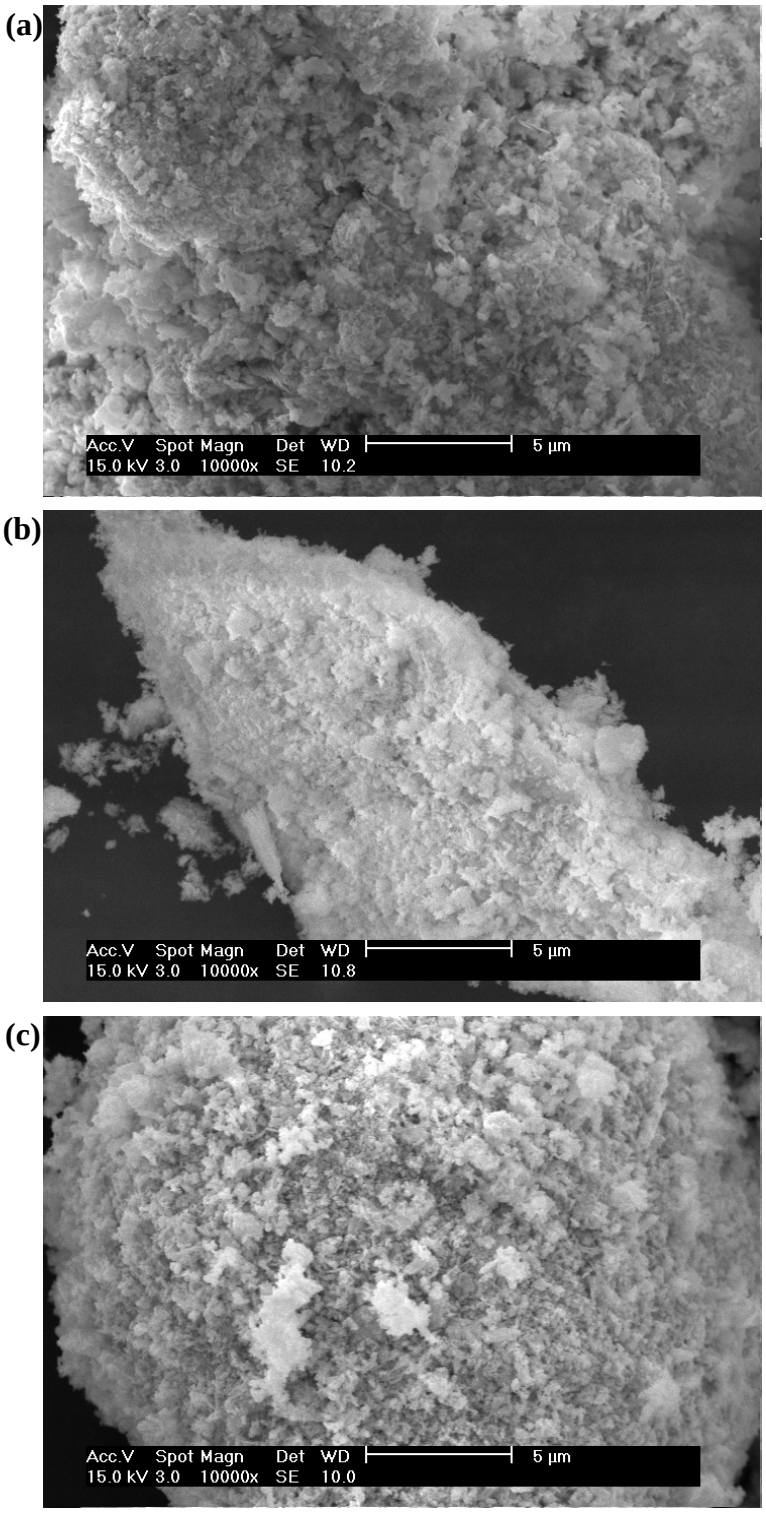

Appendix Figure 10 SEM micrographs of $Ce_{0.80}Gd_{0.20}O_{2-\delta}$ powders calcined for 2 h in air at (a) 600°C, (b) 800°C, and (c) 1000°C

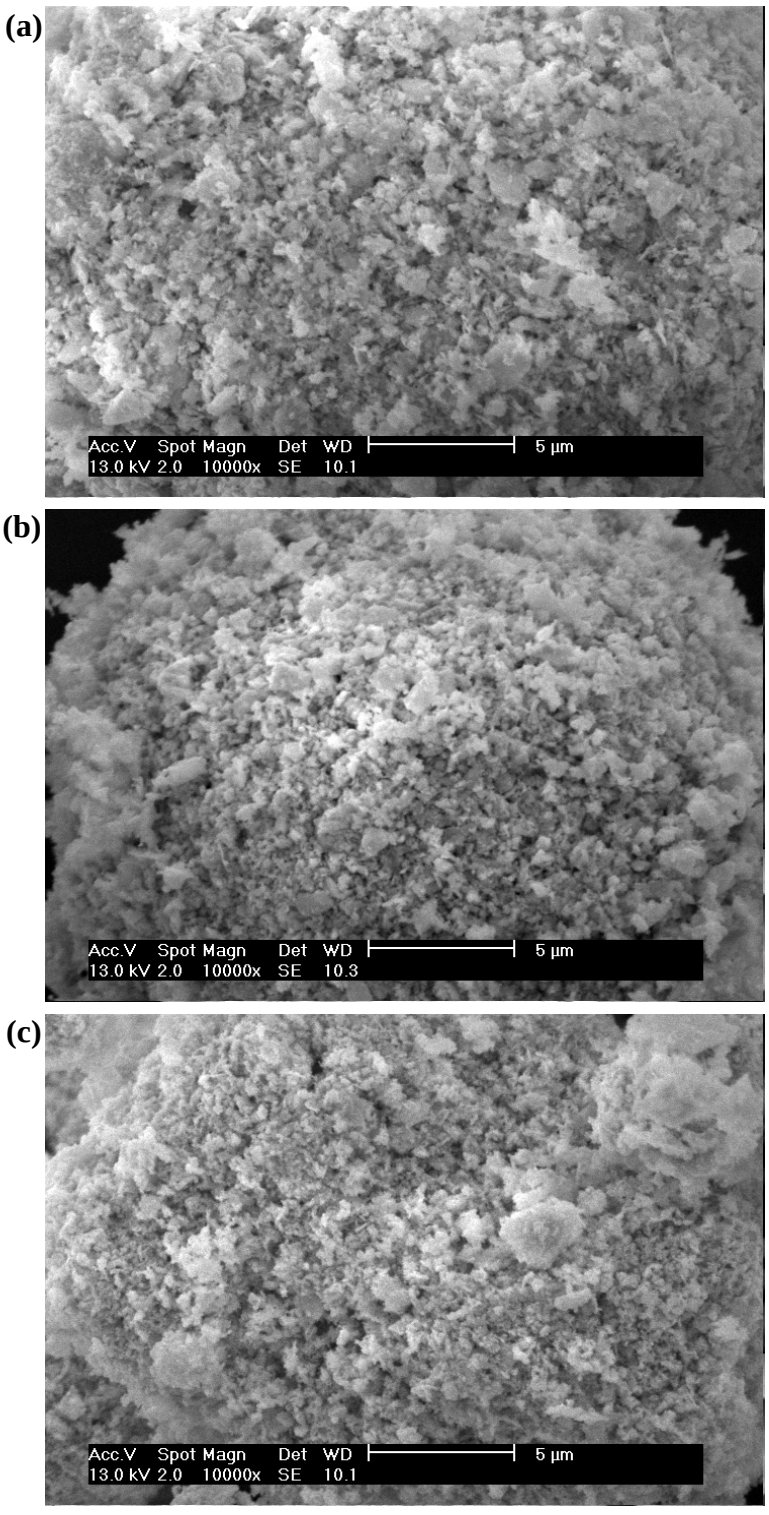

Appendix Figure 11 SEM micrographs of $Ce_{0.85}Sm_{0.15}O_{2-\delta}$ powders calcined for 2 h in air at (a) 600°C, (b) 800°C, and (c) 1000°C

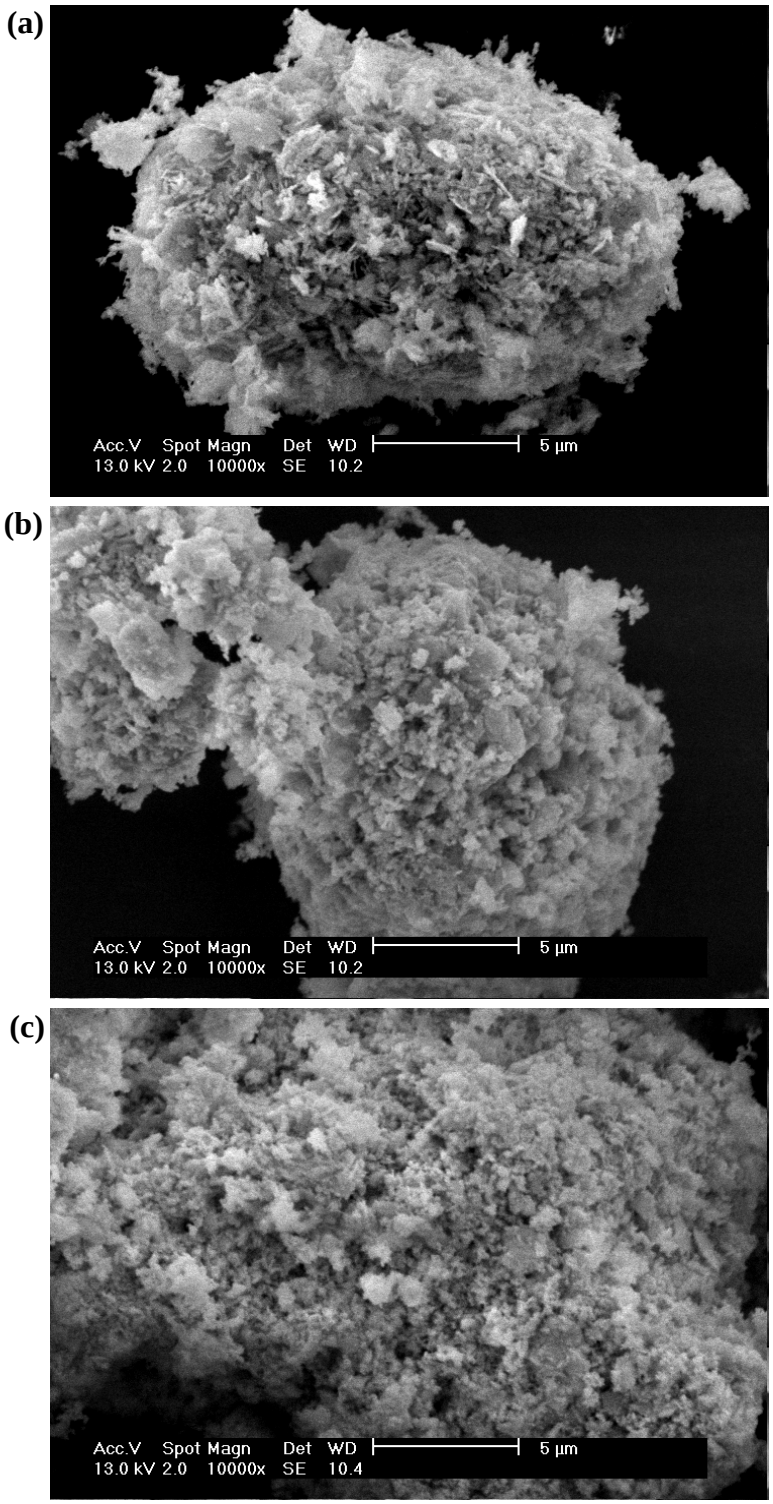

Appendix Figure 12 SEM micrographs of $Ce_{0.80}Sm_{0.20}O_{2-\delta}$ powders calcined for 2 h in air at (a) 600°C, (b) 800°C, and (c) 1000°C

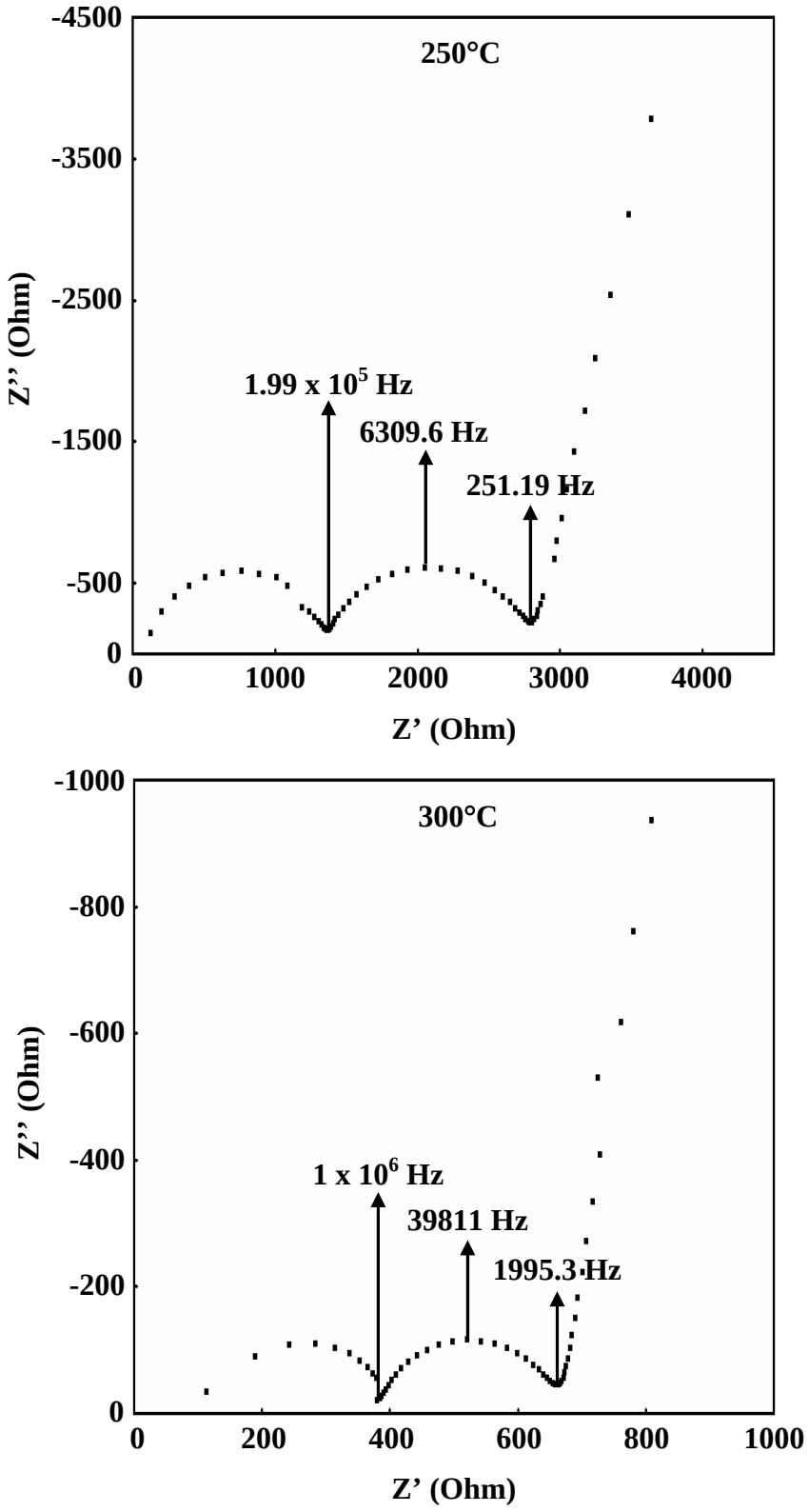

Appendix Figure 13 Impedance spectra of $Ce_{0.90}Gd_{0.10}O_{2-\delta}$ pellet which calcined at 600°C for 2 h in air and sintered at 1500°C for 5 h in air

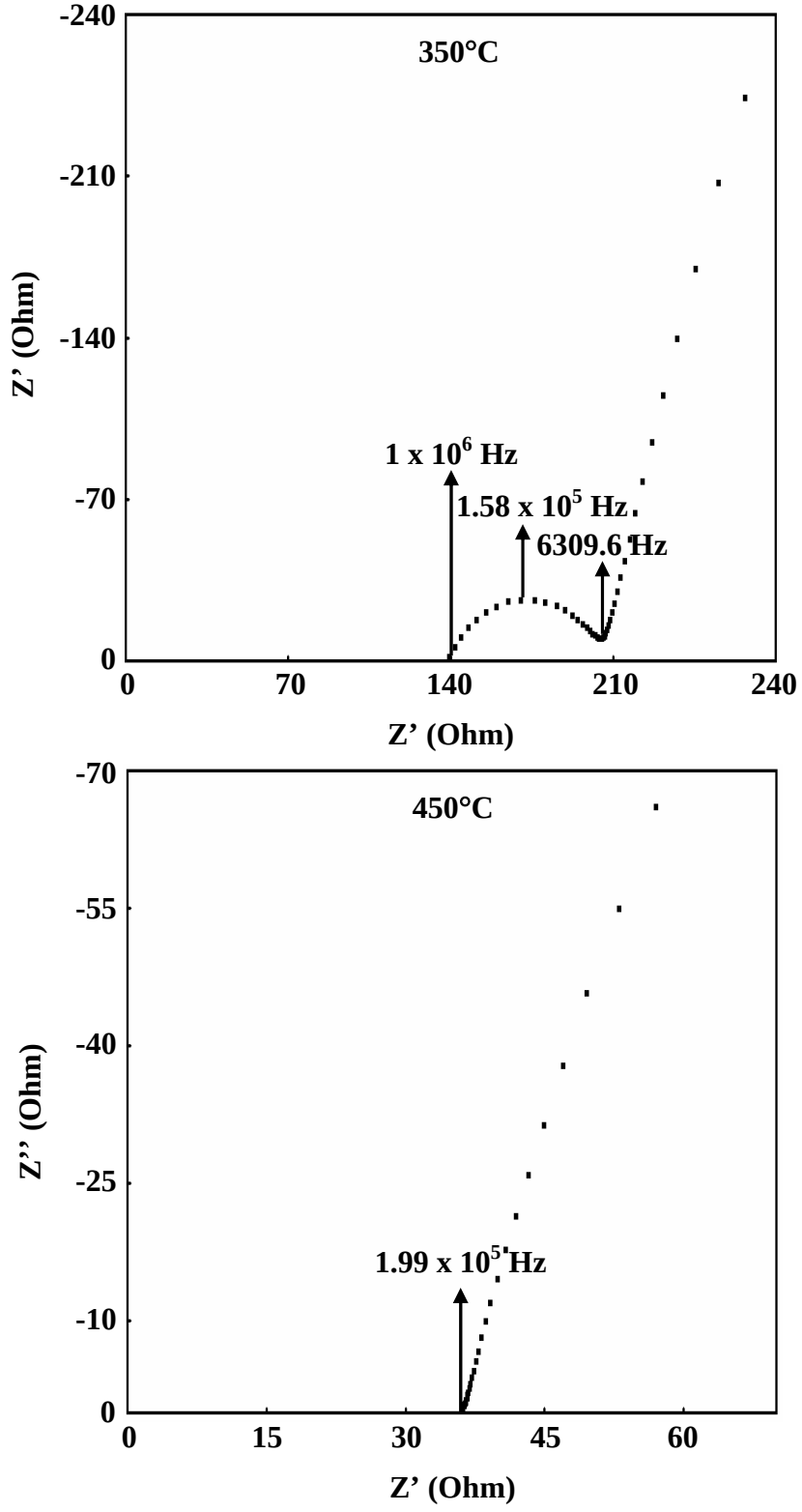

Appendix Figure 13 (Continued)

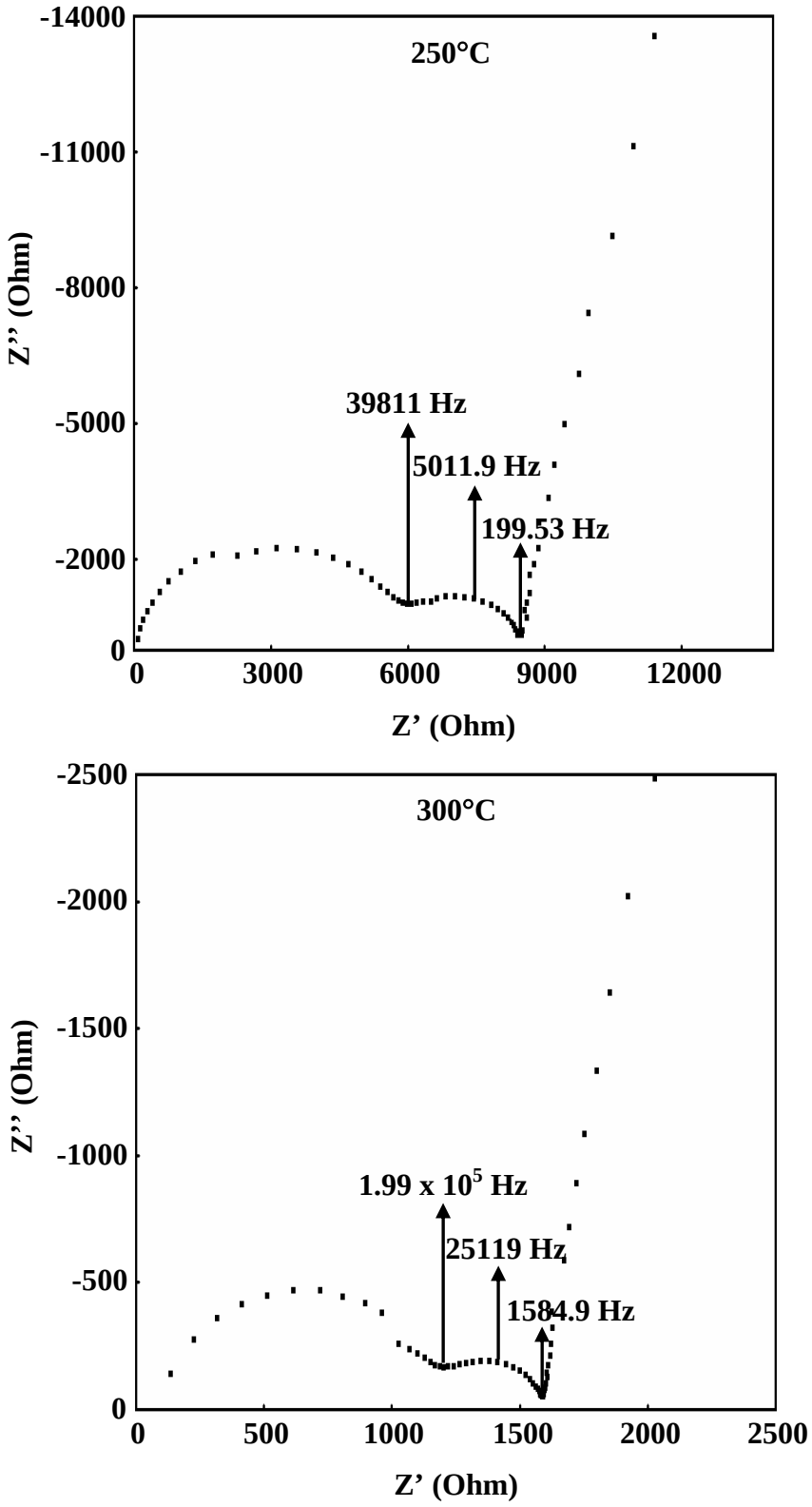

Appendix Figure 14 Impedance spectra of $Ce_{0.80}Gd_{0.20}O_{2-\delta}$ pellet which calcined at 600°C for 2 h in air and sintered at 1500°C for 5 h in air

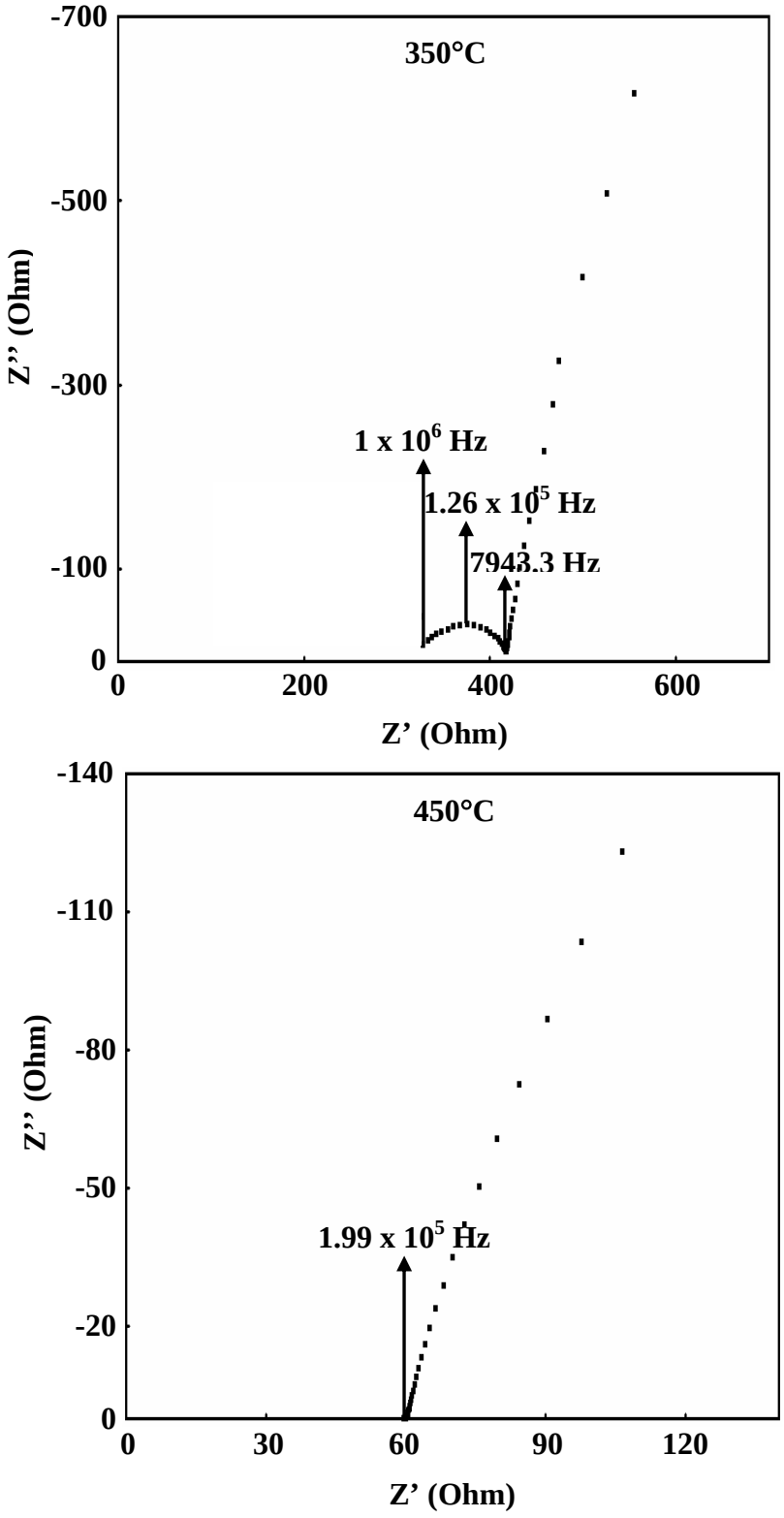

Appendix Figure 14 (Continued)

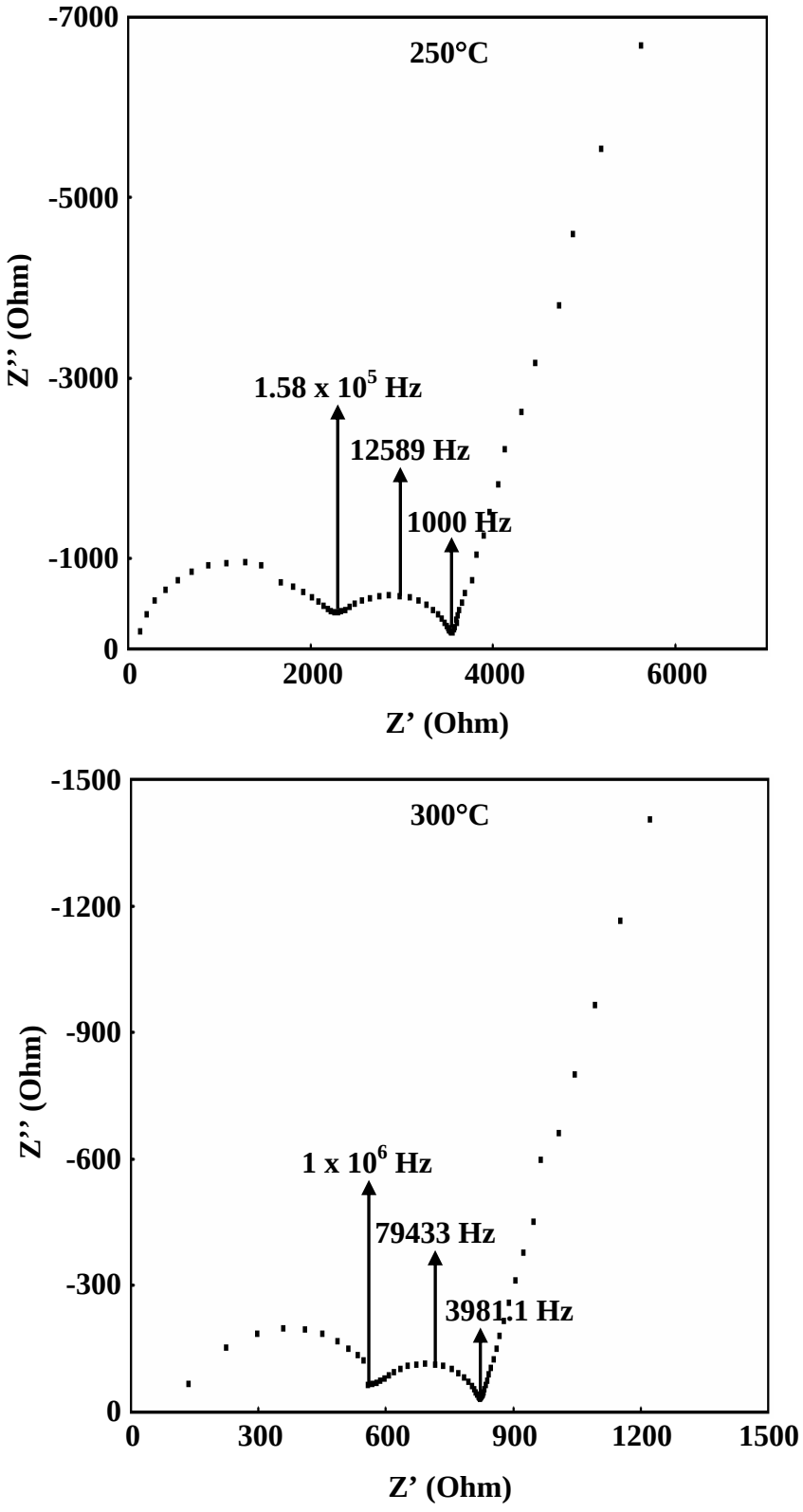

Appendix Figure 15 Impedance spectra of $Ce_{0.85}Sm_{0.15}O_{2-\delta}$ pellet which calcined at 600°C for 2 h in air and sintered at 1500°C for 5 h in air

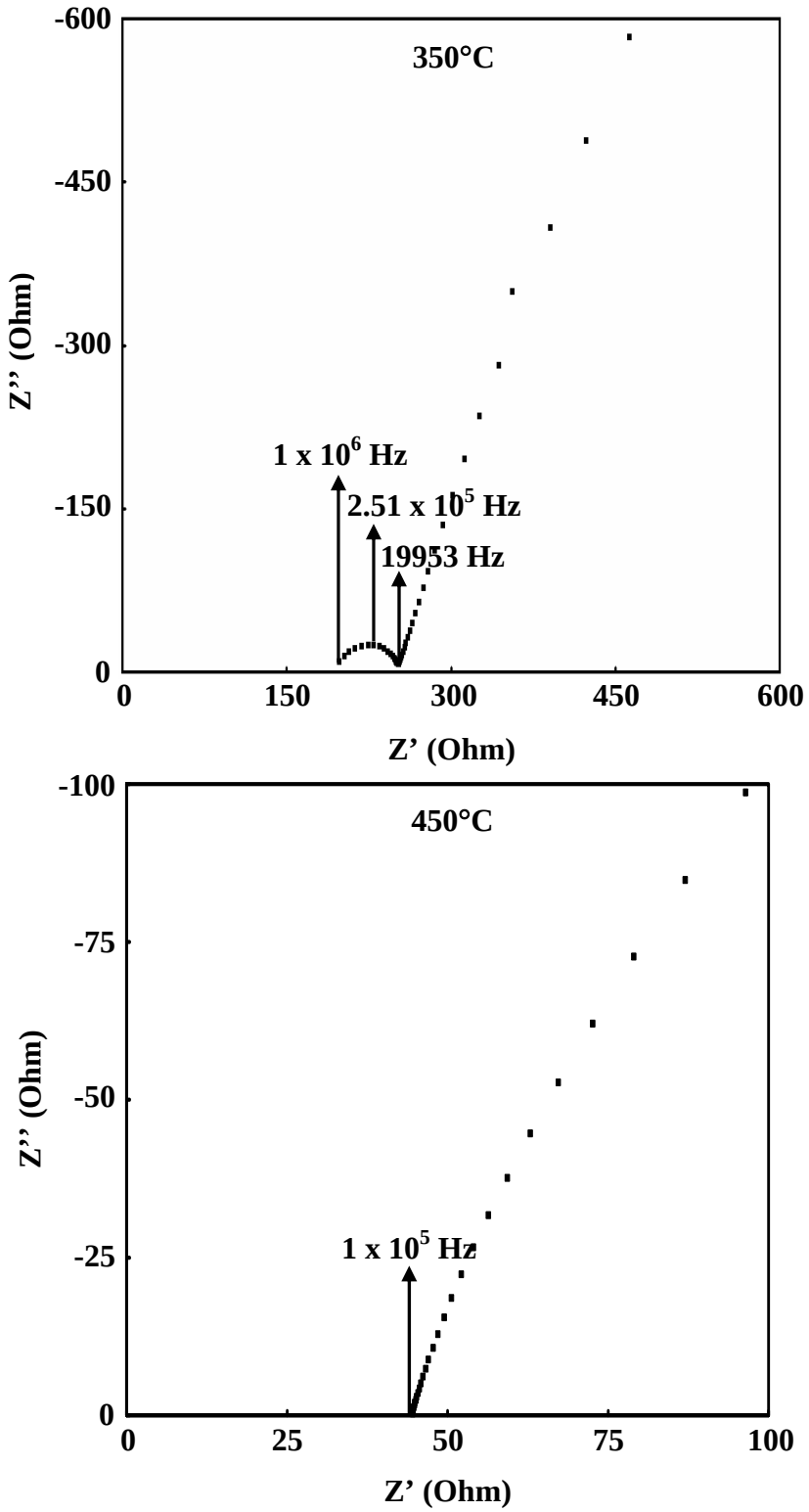

Appendix Figure 15 (Continued)

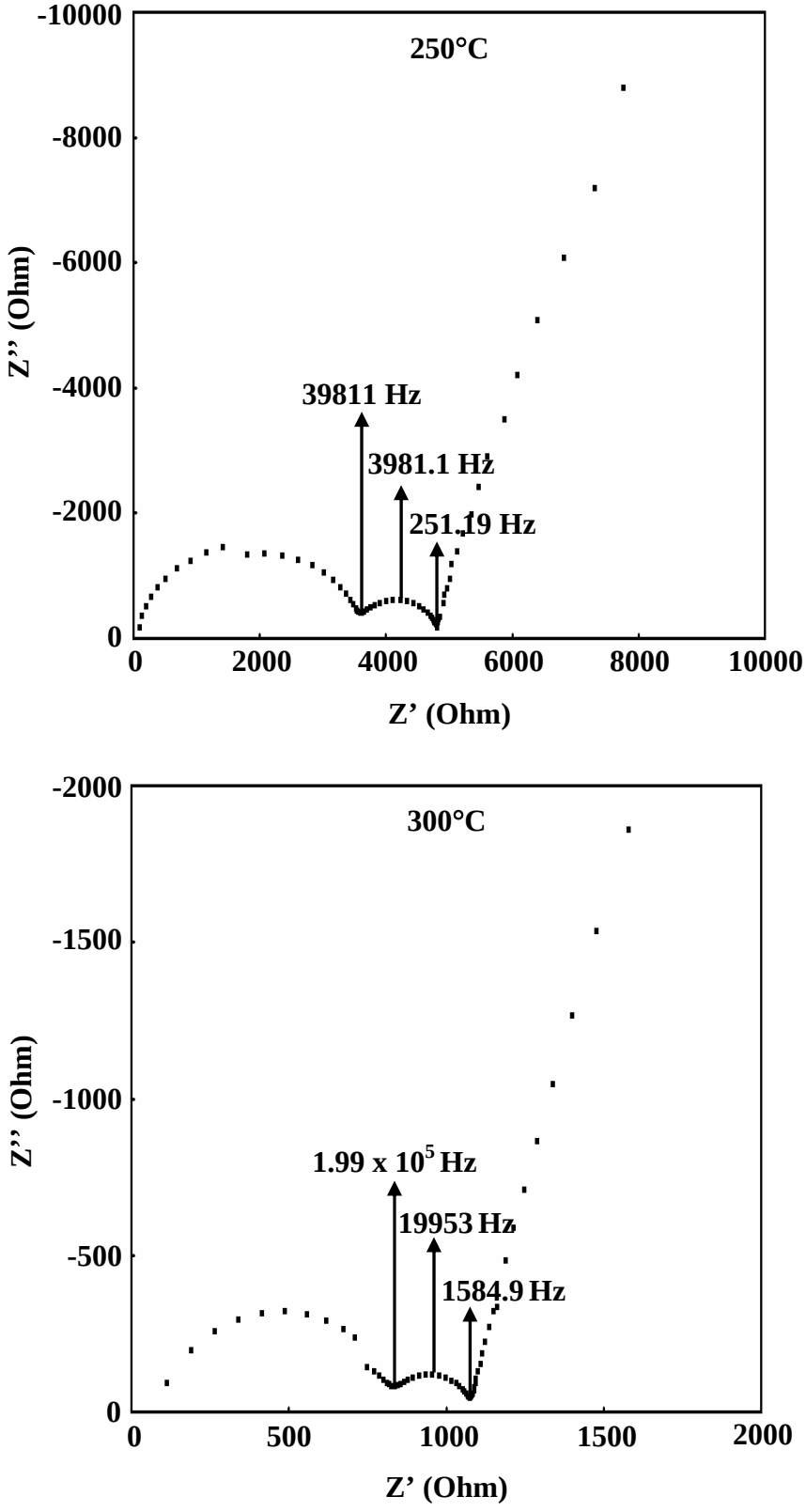

Appendix Figure 16 Impedance spectra of $Ce_{0.80}Sm_{0.20}O_{2-\delta}$ pellet which calcined at 600°C for 2 h in air and sintered at 1500°C for 5 h in air

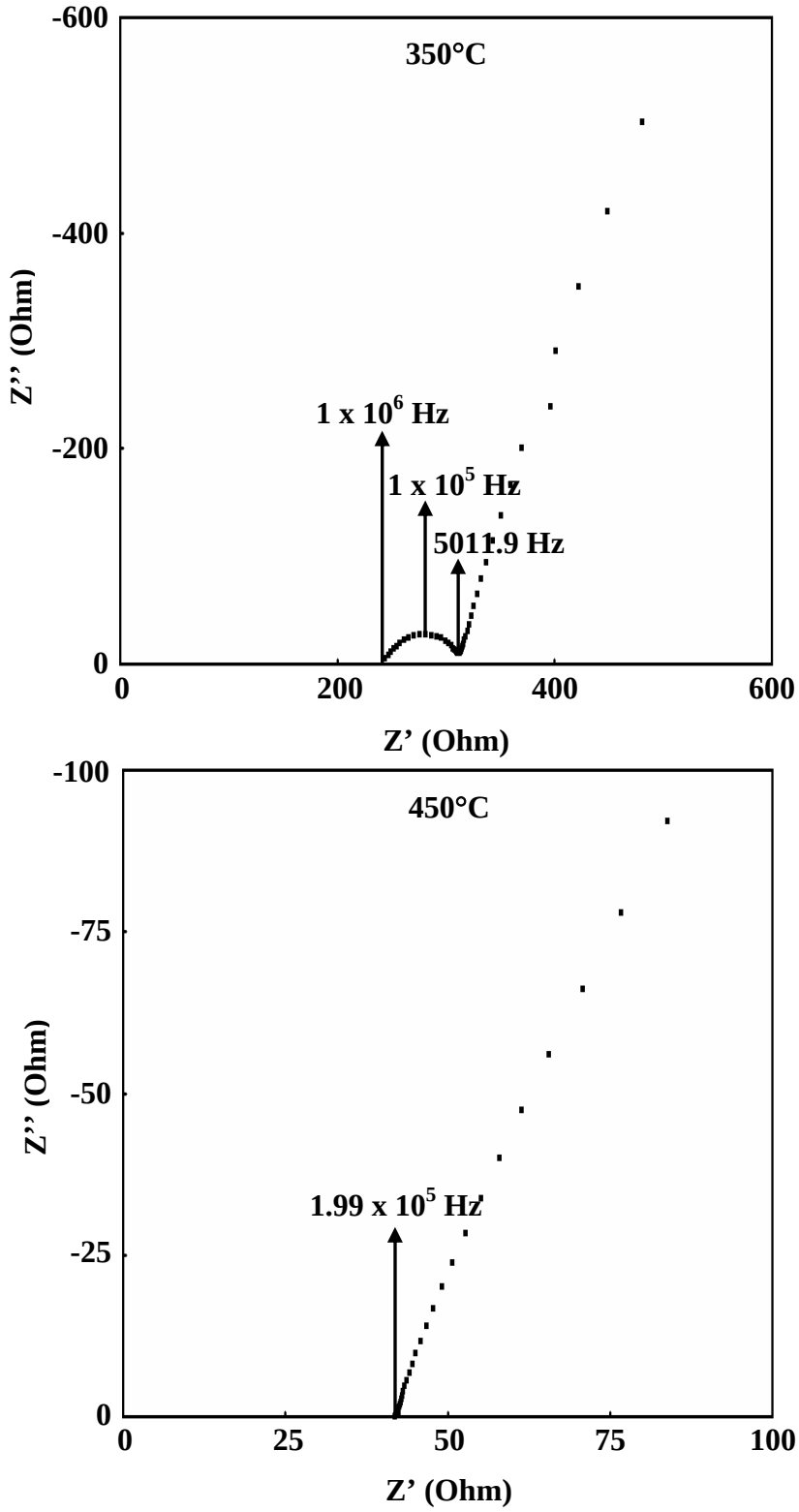

Appendix Figure 16 (Continued)

CIRRICULUM VITAE

NAME : Mr. Thamrong Rakthin

BIRTH DATE : December 10, 1984

BIRTH PLACE : Kanchanaburi, Thailand

EDUCATION :	**YEAR**	**INSTITUTE**	**DEGREE/DIPLOMA**
	2007	KMUTT	B.Sc. (Chemistry)

POSITION/TITLE : Postgraduated student

WORK PLACE : Faculty of Engineering, Kasetsart University

SCHOLARSHIP/AWARDS :
- Scholarship from Energy Policy and Planning Office (EPPO), Ministry of Energy, Thailand
- The Outstanding Poster Award from Pure and Applied Chemistry International Conference 2008 (PACCON 2008), Bangkok, Thailand